LATERAL VIBRATION OF THIN BEAM UNDER VERTICAL EXCITATION

by

VIVEKANANDA MUKHOPADHYAY
B. Tech., Indian Institue of Technology, Kharagpur
(1968)

SUBMITTED IN PARTIAL FULFILLMENT
OF THE REQUIREMENTS FOR THE
DEGREE OF MASTER OF SCIENCE

at the

MASSACHUSETTS INSTITUTE OF TECHNOLOGY
June 1970

Signature of Author_____
Department of Aeronautics
and Astronautics, June 6, 1970

Certified by

Thesis Supervisor

Accepted by_____
Chairman, Departmental
Graduate Committee

LATERAL VIBRATION OF THIN BEAM UNDER VERTICAL EXCITATION

by

Vivekananda Mukhopadhyay

Submitted to the Department of Aeronautics and Astronautics on June 6, 1970 in partial fulfillment of the requirements for the degree of Master of Science.

ABSTRACT

The dynamics of lateral bending and torsion vibration of a thin flexible beam under vertical harmonic excitation has been investigated theoretically and experimentally. Only linear theory is considered for theoretical analysis.

The governing equations are a set of coupled Mathieu type equations. Initial built-in deflections introduce forcing terms resulting in coexistence of parametric and forced excitation. The instability regions and steady state solutions are studied here.

Experimentally, the beam was excited and transient and steady state records were obtained. Three regions of instability were observed, only one of which is a linear phenomenon and agrees well with the theoretical results. The other two regions have large bending and torsion amplitudes and exhibit limit cycle type behavior. Also, peculiar snapping and whipping motions were observed. An elaborate nonlinear analysis is required to explain the later experimental results which are presented in detail.

Thesis Supervisor: John Dugundji

Title: Associate Professor of Aeronautics and Astronautics

ACKNOWLEDGEMENTS

The author wishes to acknowledge with gratitude the time and effort devoted by Professor John Dugundji who suggested the problem, provided continuous guidance and spent long hours helping in the experiment.

Sincere appreciation is extended to the Department of Aeronautics and Astronautics of MIT for the research assistantship.

The author is also indebted to his parents for their continuous encouragement throughout his study.

Finally, thanks are due to Messrs. F. Merlis, A. Shaw, J. Barley, O. Wallin for helping set up the experiment and to Miss M. Bryant for her excellent typing.

TABLE OF CONTENTS

LIST OF SYMBOLS

a_1, a_2	Dimensionless frequency parameters (Eq. 2.15)
$\bar{A}_1$, $\bar{B}_1$, $\bar{B}_{01}$	Coefficients of assumed solutions (Eq. 2.20 and 2.23)
$\bar{A}_2$, $\bar{B}_2$, $\bar{B}_{02}$	
$\bar{A}_\alpha$, $\bar{B}_\alpha$, $\bar{B}_{0\alpha}$	
$\tilde{A}_1$, $\tilde{B}_1$, $\tilde{B}_{01}$	Coefficients of assumed solutions (Eq. 2.26)
$\tilde{A}_2$, $\tilde{B}_2$, $\tilde{B}_{02}$	
$\tilde{A}_\alpha$, $\tilde{B}_\alpha$, $\tilde{B}_{0\alpha}$	
b	Thickness of the beam
B_B	Dimensionless built-in bending amplitude
B_S	" static bending amplitude (Eq. B.2)
A_1, B_1, C_1	Constants defined in Eq. (B.1)
A_2, B_2, C_2	
C_{S1}, C_{S2}	
$[C_1]$, $[C_2]$	Matrices defined in Eq. (2.21) and (2.24)
C_{V1}, C_{V2}, C_θ	Modal damping coefficients
d	Width of the beam
D	Constant defined in Eq. (B.1)
E	Modulus of elasticity
F_1	Dimensionless self weight (Eq. 2.15)

F_2	Defined in Eq. (2.15)
F_{1S}	Dimensionless static buckling self-weight
g	Acceleration due to gravity
G	Shear modulus
$h_1(\eta)$, $h_2(\eta)$	Dimensionless bending mode shapes*
$h_D(\eta,t)$	" dynamic bending deflection
$h_S(\eta)$	" static equilibrium position
H	Constant defined in Eq. (B.1)
I	Area moment about Z axis
I_m	Mass-rotary inertia about X axis
J	Polar area-moment about X axis
K_1	Dimensionless constant (Eq. 2.15)
ℓ	Length of the beam
m	Mass per unit length
M_{XO}, M_{YO}, M_{ZO}	External moments about X_0, Y_0, Z_0 axes
M_X, M_Y, M_Z	" " " X, Y, Z axes
P(s)	Distributed vertical load
P_1,...P_8	Defined in Eq. (2.30)
q_1, q_2, q_α	Dimensionless generalized coordinates*
r_1	" torsion natural frequency (Eq. 2.15)

r_2	Defined in Eq. (2.15)
s	Length coordinate along the beam
S	Constant defined in Eq. (B.1)
$[S_1]$, $[S_2]$	Matrices defined in Eq. (2.21) and (2.24)
t	Time in seconds
T_B	Dimensionless built-in twist amplitude
T_S	" static twist amplitude (Eq. B.2)
U_B	Amplitude of base motion in inches
U_{1B}	Dimensionless amplitude of base motion
U_{2B}	Defined in Eq. (2.15)
V(s,t)	Total bending deflection
$V_B(s)$	Built-in bending deflection
$V_D(s,t)$	Dynamic bending deflection
$V_S(s)$	Static bending equilibrium position
V_T	Value of V_D at tip of the beam
W_F	Forcing frequency
W_{1h}, W_{2h}	Bending mode natural frequencies*
W_α	First torsion mode natural frequency
x	Length coordinate along X_o axis
X_o, Y_o, Z_o	Undeformed axes system
X, Y, Z	Deformed axes system

$[Z_1]$, $[Z_2]$	Matrices defined in Eq. (2.21) and (2.24)
$\alpha(\eta)$	First torsion mode shape
ζ_1, ζ_2, ζ_α	Modal critical damping ratios*
$\theta(s,t)$	Total torsion in radians
$\theta_B(s)$	Built-in twist in radians
$\theta_D(s,t)$	Dynamic torsional deflection in radians
$\theta_S(s)$	Static torsion equilibrium position in radians
θ_T	Value of θ_D at tip of the beam
η	Dimensionless length coordinate = s/ℓ
σ	Complex constant (Eq. 2.20 and 2.23)
τ	Dimensionless time = $(W_F/2)t$
ξ	Dummy variable of integration
$(\dot{})$	Time derivative
$(^\circ)$	Dimensionless time derivative
$(\,)'$	Derivative w.r.t. s
$(\,)'$	Derivative w.r.t. η

*1, 2 and α refers to 1st bending, 2nd bending and 1st torsion modes respectively.

CHAPTER 1

INTRODUCTION

Parametric excitation, characterized by the variation of a parameter in an equation has been well known and was studied in detail by many authors. Bolotin[1] has investigated the application of parametric excitation to structural systems.

The physical nature of parametric excitation and of more familiar forced excitation may be distinguished by the facts that (1) for linear, low damped systems, the parametric oscillations occur over a continuous range of forcing frequencies of the varying parameter, where as the forced oscillations have the resonance behavior only at discrete values of the forcing frequency, and (2) for a simple pendulum and for a flexible beam, the parametric oscillations occur in the direction normal to the excitation, while the forced oscillations take place in the direction of the excitation. Both parametric and forced excitation can exist together in a system. A simple pendulum whose pivot point is oscillated along a line which is tilted at an angle to the vertical, receives both kinds of excitation. Linear and nonlinear analysis of such phenomena has been done in detail for both pure parametric excitation and combined parametric-forced excitation by Dugundji and Chhatpar[2,3] and provides a background for the present study.

A thin flexible cantilever beam whose base is oscillated vertically in the plane of the web which is also the plane of largest rigidity, experiences a periodic load which appears as a parametric term in the out-of-plane bending-torsion equilibrium equation. In the static case, the consideration of small lateral deflection under vertical load leads to the static stability problem. Analogous to the pendulum problem, if the beam has an initial static deflection due to built-in imperfections or if the web is initially tilted from vertical, forcing functions appear in the dynamic equilibrium equations and both parametric and forced excitation occur simultaneously. After applying Galerkin's technique with assumed normal mode shapes as weighting functions, a set of coupled equations are obtained for the time domain analysis. These equations have the same characteristics as the Mathieu equation and have been analyzed in detail by Bolotin[1] but no experimental results are presented. The present report investigates the problem of lateral vibration of thin beam both theoretically and experimentally. Only the linear theory for small motion is considered and presented in Chapter 2. The experimental investigation is presented in Chapter 3. A representative experimental observation is tabulated in Table 2. Three regions of instability were observed only one of which is a linear phenomenon and agrees well with theoretical results and is described at the end of Chapter 2. The other two regions have large bending and torsion amplitudes and exhibit limit cycle

type behavior. Also peculiar snapping and whipping motions are observed. An elaborate nonlinear analysis is required to explain the later experimental results which are presented in detail. Bolotin[1] briefly discusses the nonlinear problem but the solution is inadequate to explain them. The nonlinearities are not quite well defined and further work is required in this direction.

CHAPTER 2

THEORETICAL ANALYSIS

2.1 Mathematical Formulation

The beam shown in Fig. 4, which has an initial built-in deflection and twist V_B, θ_B with no stress developed, assumes a position V_s, θ_s after static deflection under self-weight. The final state V, θ indicates position due to dynamic loading at any instant of time. All external forces P(s) are acting in Z_o direction. Thus moments acting in X_o, Y_o, Z_o directions at a distance s from the root on the beam neutral axis are

$$\begin{aligned} M_{xo} &= \int_s^\ell P(\xi)\left[V(\xi) - V(s) \right] d\xi \\ M_{Yo} &= \int_s^\ell P(\xi)\left[\chi(\xi) - \chi(s) \right] d\xi \\ M_{zo} &= 0 \end{aligned} \tag{2.1}$$

in a right-hand system where V(s) is the position coordinate of the neutral axis in the Y_o direction, $\chi(s)$ is the coordinate in X_o direction of the point s under consideration and ℓ is the length of the beam. Resolving the moments in the deformed direction XYZ (Fig. 4) one gets under small deflection assumption

$$
\begin{aligned}
M_X &= M_{XO} + \frac{\partial V}{\partial S} M_{YO} \\
M_Y &= M_{YO} - \frac{\partial V}{\partial S} M_{XO} + \theta M_{ZO} \\
M_Z &= M_{ZO} - \theta M_{YO}
\end{aligned}
\tag{2.2}
$$

where θ is the total twist about neutral X axis measured from vertical direction in the right hand system. Since the beam is considered infinitely rigid in Z direction compared to Y direction because of its shape, the deflection in Z direction have been neglected in such a vector transformation. Since only the linear equations will be formulated here one can write $x \simeq s$ and take deflections in the deformed direction same as in the undeformed direction. Thus using the engineering bending and St. Venant torsion theory neglecting warping the static moment equilibrium equations in Z and X directions become

$$
EI \frac{\partial^2 (V - V_B)}{\partial s^2} = M_Z \tag{2.3}
$$

$$
GJ \frac{\partial (\theta - \theta_B)}{\partial s} = M_X \tag{2.4}
$$

where EI is the flexural stiffness about Z axis and GJ is the torsional stiffness about X axis.

To obtain the force equilibrium equations for the dynamic problem, one differentiates Eq. (2.3) twice and Eq. (2.4) once with respect to s and introduces inertia and damping terms

appropriately. If the base of the beam is given an acceleration $\ddot{U}_B$ in Z_o direction, the loading term P(s) becomes

$$P(s) = m(g - \ddot{U}_B) \tag{2.5}$$

where m is mass per unit length, g is acceleration due to gravity and $\dot{(\ )}$ is the time derivative $\frac{\partial(\ )}{\partial t}$. Thus the dynamic force equilibrium equations can be written as

$$EI\frac{\partial^4(V-V_B)}{\partial s^4} - \frac{m}{2}(g-\ddot{U}_B)\left[(\ell-s)^2\theta\right]'' + m\ddot{V}_D + C_V\dot{V}_D = 0 \tag{2.6}$$

$$GJ\frac{\partial^2(\theta-\theta_B)}{\partial s^2} + \frac{m}{2}(g-\ddot{U}_B)\left[(\ell-s)^2 V''\right] - I_m\ddot{\theta}_D - C_\theta\dot{\theta}_D = 0 \tag{2.7}$$

where I_m is the rotary moment of inertia per unit length about X axis, C_V and C_θ are bending and torsion damping coefficients respectively. The $(\ )'$ represent $\frac{\partial(\ )}{\partial s}$. By definition $V = V_D+V_S$, $\theta = \theta_D+\theta_S$, where V_S and θ_S represent the static equilibrium position coordinates; V_D and θ_D are the deflection and twist measured from the static equilibrium position. Subtracting the static equilibrium equations

$$EI\frac{\partial^4(V_S-V_B)}{\partial s^4} - \frac{m}{2}g\left[(\ell-s)^2\theta\right]'' = 0 \tag{2.8}$$

$$GJ\frac{\partial^2(\theta_S-\theta_B)}{\partial s^2} + \frac{m}{2}g\left[(\ell-s)^2 V''\right] = 0 \tag{2.9}$$

from Eq. (2.6) and (2.7) the following equations are obtained.

$$EI\frac{\partial^4 V_D}{\partial s^4} - \frac{m}{2}(g-\ddot{U}_B)\left[(\ell-s)^2\theta_D\right]'' + \frac{m\ddot{U}_B}{2}\left[(\ell-s)^2\theta_S\right]'' + m\ddot{V}_D + C_V\dot{V}_D = 0 \tag{2.10}$$

$$GJ\frac{\partial^2\theta_D}{\partial s^2} + \frac{m}{2}(g-\ddot{U}_B)\left[(\ell-s)^2 V_D''\right] - \frac{m\ddot{U}_B}{2}\left[(\ell-s)^2 V_S''\right] - I_m\ddot{\theta}_D - C_\theta\dot{\theta}_D = 0 \tag{2.11}$$

Nondimensionalizing by writing $\eta = s/\ell$, $h_D = V_D/\ell$, $h_S = V_S/\ell$ after rearrangement

$$\ddot{h}_D + \frac{C_V}{m}\dot{h}_D + \frac{EI}{m\ell^4}\frac{\partial^4 h_D}{\partial\eta^4} - \frac{(g-\ddot{U}_B)}{2\ell}\left[(1-\eta)^2\theta_D\right]'' = -\frac{\ddot{U}_B}{2\ell}\left[(1-\eta)^2\theta_S\right]'' \tag{2.11}$$

$$\ddot{\theta}_D + \frac{C_\theta\dot{\theta}_D}{I_m} - \frac{GJ}{I_m\ell^2}\frac{\partial^2\theta_D}{\partial\eta^2} - \frac{m\ell}{2I_m}(g-\ddot{U}_B)\left[(1-\eta)^2 h_D''\right] = -\frac{m\ell}{2I_m}\ddot{U}_B\left[(1-\eta)^2 h_S''\right] \tag{2.12}$$

where $()' = \frac{\partial()}{\partial\eta}$.

We introduce

$$h_D(\eta, t) = \sum_{n=1}^{2} h_n(\eta)\, q_n(t)$$
$$\theta_D(\eta, t) = \alpha(\eta)\, q_\alpha(t) \qquad (2.13)$$

where the assumed mode shapes $h_n(\eta)$, $\alpha(\eta)$ satisfy all boundary conditions (Appendix A). We take only the first torsion mode and first and second bending modes since they are the only dominant modes encountered in the experiment. Applying Galerkin's technique namely multiplying Eq. (2.11) by $h_1(\eta)$ and $h_2(\eta)$ successively and Eq. (2.12) by $\alpha(\eta)$ and integrating w.r.t. η from 0 to 1 we get the modal equations

$$\ddot{q}_1 + \frac{C_{V1}}{m}\dot{q}_1 + \frac{EI\ B_1}{m\ell^4 A_1} q_1 - \frac{(g-\ddot{U}_B)C_1}{2\ell\ A_1} q_\alpha = -\frac{\ddot{U}_B}{2\ell}\frac{C_{S1}}{A_1} \qquad (2.14a)$$

$$\ddot{q}_2 + \frac{C_{V2}}{m}\dot{q}_2 + \frac{EI\ B_2}{m\ell^4 A_2} q_2 - \frac{(g-\ddot{U}_B)C_2}{2\ell\ A_2} q_\alpha = -\frac{\ddot{U}_B C_{S2}}{2\ell\ A_2} \qquad (2.14b)$$

$$\ddot{q}_\alpha + \frac{C_\theta}{I_m}\dot{q}_\alpha + \frac{GJ\ H}{I_m \ell^2 D} q_\alpha - \frac{m\ell^2}{I_m D}\cdot\frac{(g-\ddot{U}_B)}{2\ell}[C_1 q_1 + C_2 q_2]$$
$$= -\frac{m\ell^2}{I_m D}\frac{\ddot{U}_B}{2\ell} S \qquad (2.14c)$$

The new symbols A_1, B_1, C_1, H, D, etc. are constants and are

defined in the Appendix B. Also because of orthogonality of the assumed mode shapes $\int_0^1 h_1 h_2 \, d\eta = 0 \quad \int_0^1 h_1'' h_2'' \, d\eta = 0$; consequently there is no coupling between q_1 and q_2 in Eq. (2.14a) and (2.14b), if one uses modal damping coefficients. Denoting

$$\frac{EI\,B_1}{m\ell^4 A_1} = \omega_{1h}^2 \qquad \frac{C_{v1}}{m} = 2\zeta_1 \omega_{1h}$$

$$\frac{EI\,B_2}{m\ell^4 A_2} = \omega_{2h}^2 \qquad \frac{C_{v2}}{m} = 2\zeta_2 \omega_{2h}$$

$$\frac{GJ\,H}{I_m \ell^2 D} = \omega_\alpha^2 \qquad \frac{C_\theta}{I_m} = 2\zeta_\alpha \omega_\alpha$$

$$\left(\frac{2\omega_{1h}}{\omega_F}\right)^2 = a_1 \qquad \left(\frac{2\omega_{1h}}{\omega_F}\right)^2 = a_2$$

$$\left(\frac{\omega_\alpha}{\omega_{1h}}\right)^2 = r_1 \qquad \left(\frac{\omega_\alpha}{\omega_{2h}}\right)^2 = \frac{a_1 r_1}{a_2} = r_2$$

$$\frac{gC_1}{2\ell\omega_{1h}^2} = F_1 \qquad \frac{gC_2}{2\ell\omega_{2h}^2} = \frac{a_1 C_2}{a_2 C_1} F_1 = F_2$$

$$\frac{U_B C_1}{\ell} = U_{1B} \qquad \frac{U_B C_2}{\ell} = \frac{U_{1B} C_2}{C_1} = U_{2B}$$

$$T_S = \frac{C_{S1}}{C_1} = \frac{C_{S2}}{C_2} \qquad B_S = \frac{S}{C_1}$$

$$K_1 = \frac{m\ell^2}{I_m D} \qquad (2.15)$$

and introducing

$$U_B = U_B \cos \omega_F t \tag{2.16}$$

$$\omega_F t = 2\tau \tag{2.17}$$

for harmonic base motion with amplitude U_B and forcing frequency W_F and nondimensional time τ we get the equations in their final form

$$\ddot{q}_1 + 2\zeta_1\sqrt{a_1}\,\dot{q}_1 + a_1 q_1 - [a_1 F_1 + 2U_{1B}\cos 2\tau]\,q_\alpha = 2U_{1B} T_S \cos 2\tau \tag{2.18a}$$

$$\ddot{q}_2 + 2\zeta_2\sqrt{a_2}\,\dot{q}_2 + a_2 q_2 - [a_2 F_2 + 2U_{2B}\cos 2\tau]\,q_\alpha = 2U_{2B} T_S \cos 2\tau \tag{2.18b}$$

$$\ddot{q}_\alpha + 2\zeta_\alpha\sqrt{a_1 r_1}\,\dot{q}_\alpha + a_1 r_1 q_\alpha - K_1[a_1 F_1 + 2U_{1B}\cos 2\tau]\,q_1 - K_1[a_2 F_2 + 2U_{2B}\cos 2\tau]\,q_2 = 2K_1 U_{1B} B_S \cos 2\tau \tag{2.18c}$$

where $(\dot{}) = \frac{\partial()}{\partial}$ and we have introduced the values $A_1 = A_2 = 1$. One can write $a_2 r_2$ in place of $a_1 r_1$ since they both denote $(2W_\alpha / W_F)^2$.

2.2 Pure Parametric Excitation

If the right hand side forcing terms originating from initial static deflection are set equal to zero, we get a set

of coupled equations which are similar in characteristics to the well known Mathieu Equations[1], and can be treated in a similar fashion. However, because of their complexity, it is not possible to write closed form approximate solutions. However, we shall demonstrate here how one proceeds to determine the solutions and the instability regions, when the two bending modes and one torsion mode are participating.

By going into the general theory discussed by Bolotin[1], it can be shown that certain values of W_F and U_B lead to unbounded, i.e., unstable solutions while other values lead to bounded or stable solutions. A plot of W_F versus U_B can then be constructed separating the stable and unstable regions of these equations. Such plots are shown in Fig. 5 and 6 in $W_F/2W_{1h}$ vs. U_{1B}. For small values of U_{1B}, U_{2B} various regions of instability develop near $a_1 \simeq 1, 4, 9, \ldots$ $a_2 \simeq 1, 4, 9 \ldots$ $a_1 r_1 \simeq 1, 4, 9 \ldots$ etc.

It is observed that near the second instability region at a_1, a_2, $a_1 r_1 \simeq 4$, i.e. $W_F \simeq W_{1h}$, W_{2h}, W_α respectively, there is greatest interaction between the forced and parametric excitation[3] and we obtained this in the experiment. Also for this investigation $|U_{1B}|$, $|U_{2B}| < 1$.

The homogeneous equations are

$$\ddot{q}_1 + 2\zeta_1\sqrt{a_1}\,q_1 + a_1 q_1 - \left[a_1 F_1 + 2U_{1B}\cos 2\tau\right] q_\alpha = 0 \qquad (2.19a)$$

$$\ddot{q}_2 + 2\zeta_2\sqrt{a_2}\,q_2 + a_2 q_2 - \left[a_2 F_2 + 2U_{2B}\cos 2\tau\right] q_\alpha = 0 \qquad (2.19b)$$

$$\ddot{q}_\alpha + 2\zeta_\alpha\sqrt{a_1 r_1}\,q_\alpha + a_1 r_1 q_\alpha - K_1[a_1 F_1 + 2U_{1B}\cos 2\tau]q_1$$

$$-K_1[a_2 F_2 + 2U_{2B}\cos 2\tau]q_\alpha = 0 \qquad (2.19c)$$

a) First Instability Region

In the vicinity of first instability region and for values $|U_{1B}|$, $|U_{2B}| < 0.6$ a good approximation to the solution of Eqs. (2.19) can be shown to be[2]

$$\begin{aligned} q_1 &= e^{\sigma\tau}(\bar{B}_1\cos\tau + \bar{A}_1\sin\tau) \\ q_2 &= e^{\sigma\tau}(\bar{B}_2\cos\tau + \bar{A}_2\sin\tau) \\ q_\alpha &= e^{\sigma\tau}(\bar{B}_\alpha\cos\tau + \bar{A}_\alpha\sin\tau) \end{aligned} \qquad (2.20)$$

where σ is a constant to be determined, and $\bar{A}_1$, $\bar{B}_1$ etc. are constants. Substituting Eqs. (2.20) into (2.19) and equating to zero the coefficients of $e^{\sigma\tau}\sin\tau$, $e^{\sigma\tau}\cos\tau$, and discarding $e^{\sigma\tau}\sin 3\tau$, $e^{\sigma\tau}\cos 3\tau$ terms for this approximation, we have a set of the following equations.

$$\left[\begin{array}{c|c} [C_1]_{3\times3} & [Z_1]_{3\times3} \\ \hline -[Z_1]_{3\times3} & [S_1]_{3\times3} \end{array}\right] \left\{\begin{array}{c} \bar{B}_1 \\ \bar{B}_2 \\ \bar{B}_\alpha \\ \bar{A}_1 \\ \bar{A}_2 \\ \bar{A}_\alpha \end{array}\right\} = 0 \qquad (2.21)$$

where

$$[C_1] = \begin{bmatrix} \sigma^2 + 2\zeta_1\sqrt{a_1}\,\sigma + a_1 - 1 & 0 & -(a_1F_1 + U_{1B}) \\ 0 & \sigma^2 + 2\zeta_2\sqrt{a_2}\,\sigma + a_2 - 1 & -(a_2F_2 + U_{2B}) \\ -K_1(a_1F_1 + U_{1B}) & -K_1(a_2F_2 + U_{2B}) & \sigma^2 + 2\zeta_\alpha\sqrt{a_1r_1}\,\sigma + a_1r_1 - 1 \end{bmatrix}$$

$$[S_1] = \begin{bmatrix} \sigma^2 + 2\zeta_1\sqrt{a_1}\,\sigma + a_1 - 1 & 0 & (-a_1F_1 + U_{1B}) \\ 0 & \sigma^2 + 2\zeta_2\sqrt{a_2}\,\sigma + a_2 - 1 & (-a_2F_2 + U_{2B}) \\ K_1(-a_1F_1 + U_{1B}) & K_1(-a_2F_2 + U_{2B}) & \sigma^2 + 2\zeta_\alpha\sqrt{a_1r_1}\,\sigma + a_1r_1 - 1 \end{bmatrix}$$

$$[Z_1] = \begin{bmatrix} -2(\sigma + \zeta_1\sqrt{a_1}) & 0 & 0 \\ 0 & -2(\sigma + \zeta_2\sqrt{a_2}) & 0 \\ 0 & 0 & -2(\sigma + \zeta_\alpha\sqrt{a_1r_1}) \end{bmatrix}$$

For a nontrivial solution of Eq. (2.21), the determinant $\Delta=0$. It can be shown that under slowly varying amplitude assumption a good approximation to Eq. (2.21) may be obtained by neglecting the σ^2 and σ terms in the main diagonal elements of the $[C_1]$ and $[S_1]$ matrix. Only the smallest roots of σ of the resulting determinant are applicable near the instability regions. The other roots are sensitive to the neglect of $\sin 3\tau$, $\cos 3\tau$ terms. These three values constitute the three independent solutions of the form of Eqs. (2.20). If farther for a particular conbination of W_F and U_B the real part of the root is positive, it gives an unbounded solution and the point W_F, U_B, for given values of ζ_1, ζ_2, ζ_α is unstable. If the real part is negative, the two solutions are bounded and the point W_F, U_B is stable. The points where the real part of σ is zero define the boundary between the stable and unstable regions. To complete solution of homogeneous set of equations Eq. (2.19) one evaluates $\bar{B}_1,\bar{B}_2,\bar{B}_\alpha,\bar{A}_2,\bar{A}_\alpha$ in terms of $\bar{A}_1$ after the three values of σ has been found. Then placing these in Eq. (2.20) one obtains three independent solutions of q_1, q_2, and q_α corresponding to the three values of σ. The two arbitrary constants for each equation can then be obtained from the six initial conditions. One can obtain the stability boundary by putting $\sigma=0$ in the determinant of coefficients in Eq. (2.21). For no damping case, the determinant decouples to give two equations.

$$(a_1-1)(a_2-1)(a_1\gamma_1-1) - K_1\left\{(a_1F_1+U_{1B})^2(a_2-1) + (a_2F_2+U_{2B})^2(a_1-1)\right\} = 0$$

$$(a_1-1)(a_2-1)(a_1\gamma_1-1) - K_1\left\{(-a_1F_1+U_{1B})^2(a_2-1) + (-a_2F_2+U_{2B})^2(a_1-1)\right\} = 0$$

(2.22)

These are solved by trial and plotted in Fig. 5a in $W_F/2W_{1h}$ versus U_{1B} for which the above equations become zero. The pair of line at $W_F \simeq 2$ CPS encloses a region where the instability will be predominantly in first bending mode. This encloses a very narrow region within our operating point of base amplitudes. The pair of line at $W_F \simeq 14$ CPS encloses the second bending mode instability region. The pair of line at $W_F \simeq 34$ CPS encloses the region where the instability will be predominantly in first torsion mode. The effect of damping is to narrow down these regions farther, thus because of large damping present the first two regions were not encountered in the experiment. The beam was excited up to $W_F \simeq 30$ CPS so the experiment does not include the torsion instability region but it was observed that there is a strong instability region just beyond $W_F \simeq 30$ CPS.

Proceeding in a similar way one can determine the first instability boundaries assuming that only the first bending and first torsion modes participate in the response. This is shown in Fig. 6a. It is observed that exclusion of second bending mode does not affect the instability region near $W_F \simeq 2$ CPS but the region near $W_F \simeq 34$ CPS is considerably

narrow. Thus in the first instability region the second bending mode plays a dominant part.

b) Second Instability Region

In this region for $|U_{1B}||U_{2B}| < 1$ a good approximation to the solution of Eqs. (2.19) can be shown to be[3]

$$\begin{aligned} q_1 &= e^{\sigma\tau}(\bar{B}_{01} + \bar{B}_1 \cos 2\tau + \bar{A}_1 \sin 2\tau) \\ q_2 &= e^{\sigma\tau}(\bar{B}_{02} + \bar{B}_2 \cos 2\tau + \bar{A}_2 \sin 2\tau) \\ q_\alpha &= e^{\sigma\tau}(\bar{B}_{0\alpha} + \bar{B}_\alpha \cos 2\tau + \bar{A}_\alpha \sin 2\tau) \end{aligned} \tag{2.23}$$

where σ is a constant to be determined and $\bar{B}_{01}, \bar{B}_1$ etc. are constants. One may proceed in exactly the same way as for the first instability region, i.e. substitute Eqs. (2.23) in Eqs. (2.19) and equate to zero the coefficients $e^{\sigma\tau}$, $e^{\sigma\tau}\sin 2\tau$, $e^{\sigma\tau}\cos 2\tau$, discarding $e^{\sigma\tau}\sin 4\tau$, $e^{\sigma\tau}\cos 4\tau$ terms for this approximation, and proceed to determine σ for a nontrivial solution.

To determine the stability boundary between the divergent and convergent solution, one may proceed with $\sigma=0$ to get

$$\begin{bmatrix} [C_2]_{6\times6} & [Z_2]^T_{6\times3} \\ -[Z_2]_{3\times6} & [S_2]_{3\times3} \end{bmatrix} \begin{Bmatrix} \bar{B}_{o1} \\ \bar{B}_{o2} \\ \bar{B}_{o\alpha} \\ \bar{B}_1 \\ \bar{B}_2 \\ \bar{B}_\alpha \\ \bar{A}_1 \\ \bar{A}_2 \\ \bar{A}_\alpha \end{Bmatrix} = 0 \qquad (2.24)$$

where

$$[C_2] = \begin{bmatrix} a_1 & 0 & -a_1F_1 & 0 & 0 & -U_{1B} \\ 0 & a_2 & -a_2F_2 & 0 & 0 & -U_{2B} \\ -K_1a_1F_1 & -K_1a_2F_2 & a_1r_1 & -K_1U_{1B} & -K_1U_{2B} & 0 \\ 0 & 0 & -2U_{1B} & (a_1-4) & 0 & -a_1F_1 \\ 0 & 0 & -2U_{2B} & 0 & (a_2-4) & -a_2F_2 \\ -2K_1U_{1B} & -2K_1U_{2B} & 0 & -K_1a_1F_1 & -K_1a_2F_2 & (a_1r_1-4) \end{bmatrix}$$

$$[S_2] = \begin{bmatrix} (a_1-4) & 0 & -a_1F_1 \\ 0 & (a_2-4) & -a_2F_2 \\ -K_1a_1F_1 & -K_1a_2F_2 & (a_1r_1-4) \end{bmatrix}$$

$$[Z_2] = \begin{bmatrix} 0 & 0 & 0 & 4\zeta_1\sqrt{a_1} & 0 & 0 \\ 0 & 0 & 0 & 0 & 4\zeta_2\sqrt{a_2} & 0 \\ 0 & 0 & 0 & 0 & 0 & 4\zeta_\alpha\sqrt{a_1 r_1} \end{bmatrix}$$

For nontrivial solution, the determinant of the coefficients in Eq. (2.24) must be zero. The combination of W_F, U_B which makes it zero can then be plotted to give the stability boundary for given ζ_1, ζ_2, ζ_α. For no damping case, this determinant decouples to give two equations

$$\Delta[S_2] = (a_1-4)(a_2-4)(a_1r_1-4) - K_1(a_1F_1)^2(a_2-4) - K_1(a_2F_2)^2(a_1-4) = 0$$

$$\begin{aligned}\Delta[C_2] = {} & \Delta[S_2]\times[a_1a_2(a_1r_1) - K_1a_1(a_2F_2)^2 - K_1a_2(a_1F_1)^2] \\ & + 4K_1^2[U_{1B}^2(a_2-4) + U_{2B}^2(a_1-4)]\left[a_1U_{2B}^2 + a_2U_{1B}^2 - \frac{a_1a_2}{2K_1}(a_1r_1-4)\right] \\ & + 2K_1^2[U_{1B}a_2F_2 - U_{2B}a_1F_1]^2[a_1a_2 + (a_1-4)(a_2-4)] \\ & - 4K_1^2a_1a_2[U_{1B}F_1 + U_{2B}F_2][U_{1B}a_1F_1(a_2-4) + U_{2B}a_2F_2(a_1-4)] \\ & - 2K_1a_1r_1(a_1-4)(a_2-4)[a_1U_{2B}^2 + a_2U_{1B}^2] = 0\end{aligned}$$

(2.25)

These are solved by trial and plotted in Fig. 5b. in $W_F/2W_{1h}$ versus U_{1B} for which the above equations become zero. The second instability boundaries enclose three regions at W_F near the natural frequencies of the three modes considered here. The pairs of line at $W_F \simeq 1$ and 7 CPS enclose the regions where the instability will be predominantly in the first and second bending mode respectively. These enclose very narrow regions, and only a mild effect of the region at $W_F \simeq 7$ CPS is observed at higher base amplitudes. The pair of line at $W_F \simeq 17$ CPS encloses a very wide region where the instability will be predominantly in the first torsion mode. This region is encountered in the experiment.

Proceeding in a similar way one can determine the second instability boundaries assuming that only the first bending and first torsion modes participate in the response. This is shown in Fig. 6b. It is observed that the exclusion of second bending mode does not change the instability regions near $W_F \simeq 1$ and 17 CPS appreciably. Thus in the second instability region, the second bending mode does not play a dominant part and one can investigate by taking only the first bending and first torsion mode.

2.3 Forced Excitation

Here a particular solution of Eqs. 2.18 is desired. A particular solution is assumed of the form

$$
\begin{aligned}
q_1 &= \tilde{B}_{01} + \tilde{B}_1 \cos 2\tau + \tilde{A}_1 \sin 2\tau \\
q_2 &= \tilde{B}_{02} + \tilde{B}_2 \cos 2\tau + \tilde{A}_2 \sin 2\tau \\
q_\alpha &= \tilde{B}_{0\alpha} + \tilde{B}_\alpha \cos 2\tau + \tilde{A}_\alpha \sin 2\tau
\end{aligned} \tag{2.26}
$$

where $\tilde{B}_{01}$, $\tilde{B}_1$ are constants to be determined. Substituting this into Eq. (2.18), then matching the coefficients of constant terms, sin 2τ , cos 2τ and discarding the sin 4τ , cos 4τ terms for this approximation we get the following set of equations

$$
\left[\begin{array}{c|c}
\underset{6\times6}{[C_2]} & \underset{6\times3}{[Z_2]^T} \\
\hline
-\underset{3\times6}{[Z_2]} & \underset{3\times3}{[S_2]}
\end{array}\right]
\left\{\begin{array}{c}
\tilde{B}_{01} \\ \tilde{B}_{02} \\ \tilde{B}_{0\alpha} \\ \tilde{B}_1 \\ \tilde{B}_2 \\ \tilde{B}_\alpha \\ \tilde{A}_1 \\ \tilde{A}_2 \\ \tilde{A}_\alpha
\end{array}\right\}
=
\left\{\begin{array}{c}
0 \\ 0 \\ 0 \\ 2U_{1B}T_S \\ 2U_{2B}T_S \\ 2K_1U_{1B}B_S \\ 0 \\ 0 \\ 0
\end{array}\right\} \tag{2.27}
$$

where $[C_2]$ $[S_2]$ $[Z_2]$ are as defined in Eq. (2.24). For pure parametric excitation case $T_s = B_s = 0$ and the determinant of left hand side is set equal to zero and will yield the damped stability boundary. (It is noted that the solution of Eq. (2.26) is same as solution Eq. (2.23) when $\sigma = 0$.) For the present forced excitation case one can solve Eq. (2.27) to find the constants $\tilde{B}_{01}$, $\tilde{B}_{02}$, etc., and determine the amplitudes of steady-state oscillation.

The characteristics of the steady state soltution for small damping are apparent from the Eq. (2.26) and (2.27). The solution oscillates at the forcing frequency W_F. There is a constant center shift $\tilde{B}_{01}, \tilde{B}_{02}, \tilde{B}_{0\alpha}$. The coefficients $\tilde{B}$'s become large near the lower bounds of the instability regions and the coefficients $\tilde{A}$'s dominate the amplitude of oscillation near the upper bounds in the immediate vacinity of a_1, a_2, $a_1 r_1 \simeq 4$. The amplitudes become infinite at the stability boundaries since the determinant of coefficients is zero there. Thus infinite amplitudes appear over a finite frequency gap. However, as the damping ζ_1 ζ_2 ζ_α increases, the gap narrows and if they are high enough, the infinite amplitudes disappear.

For no damping case, $[C_2]$ and $[S_2]$ decouple and one has to solve

$$\underset{6\times6}{[C_2]} \begin{Bmatrix} \tilde{B}_{01} \\ \tilde{B}_{02} \\ \tilde{B}_{0\alpha} \\ \tilde{B}_1 \\ \tilde{B}_2 \\ \tilde{B}_\alpha \end{Bmatrix} = \begin{Bmatrix} 0 \\ 0 \\ 0 \\ 2U_{1B}T_S \\ 2U_{2B}T_S \\ 2K_1U_{1B}B_S \end{Bmatrix} \tag{2.28a}$$

and

$$\underset{3\times3}{[S_2]} \begin{Bmatrix} \tilde{A}_1 \\ \tilde{A}_2 \\ \tilde{A}_\alpha \end{Bmatrix} = \begin{Bmatrix} 0 \\ 0 \\ 0 \end{Bmatrix} \tag{2.28b}$$

to determine the amplitude of steady state oscillations. The contribution of $\tilde{A}_1$, $\tilde{A}_2$, $\tilde{A}_\alpha$, will be zero except on the upper bounds of the second instability regions of Fig. 5b where determinant of $[S_2]$ is itself zero. The solutions of Eq. (2.28a) are not valid inside the instability regions since the homogeneous solution is divergent there. Eq. (2.28a) is solved numerically and plotted in Fig. 5c over the frequency ranges of interest for a fixed base amplitude. The constant center shifts $\tilde{B}_{01}$, $\tilde{B}_{02}$, $\tilde{B}_{0\alpha}$ are of order 10^{-2} except near the instability regions.

2.4 Forced Excitation (Two Mode Approximation)

In Chapter 2.2 it was observed that the second stability regions at $W_F \tilde{=} 1$ and 17 CPS do not change appreciably if the second bending mode is excluded. Thus working with just two equations a closed form steady-state solution can be obtained which includes the damping and the experimental results can be compared. For this case, the particular solution of Eqs. (2.18a) and (2.18c) with q_2 set equal to zero is desired. This is easily obtained by contraction of Eq. (2.27) by setting $\tilde{B}_{02}$, $\tilde{B}_2$ and $\tilde{A}_2$ equal to zero and neglecting associated equations to give

$$\left[\begin{array}{cccc:cc} a_1 & -a_1F_1 & 0 & -U_{1B} & 0 & 0 \\ -K_1a_1F_1 & a_1r_1 & -K_1U_{1B} & 0 & 0 & 0 \\ 0 & -2U_{1B} & (a_1-4) & -a_1F_1 & 4\zeta_1\sqrt{a_1} & 0 \\ -2K_1U_{1B} & 0 & -K_1a_1F_1 & (a_1r_1-4) & 0 & 4\zeta_\alpha\sqrt{a_1r_1} \\ 0 & 0 & -4\zeta_1\sqrt{a_1} & 0 & (a_1-4) & -a_1F_1 \\ 0 & 0 & 0 & -4\zeta_\alpha\sqrt{a_1r_1} & -K_1a_1F_1 & (a_1r_1-4) \end{array}\right] \left\{\begin{array}{c} \tilde{B}_{01} \\ \tilde{B}_{0\alpha} \\ \tilde{B}_1 \\ \tilde{B}_\alpha \\ \tilde{A}_1 \\ \tilde{A}_\alpha \end{array}\right\} = \left\{\begin{array}{c} 0 \\ 0 \\ 2U_{1B}T_S \\ 2KU_{1B}B_S \\ 0 \\ 0 \end{array}\right\}$$

(2.29)

For pure parametric excitation case, $T_S = B_S = 0$, the determinant of left hand side is set equal to zero and will yield the damped stability boundary. For the present forced excitation case, Eq. (2.29) can be solved for $\tilde{B}_{01}, \tilde{B}_1, \tilde{A}_1, \tilde{B}_{0\alpha}, \tilde{B}_\alpha, \tilde{A}_\alpha$ to give

$$\tilde{B}_{0\alpha} = 2U_{1B}P_1\left[T_S\left(\frac{P_4}{K_1F_1} - P_5\right) - B_S(P_2 - P_3)\right] \Big/ P_8$$

$$\tilde{B}_\alpha = 2U_{1B}P_1\left[\frac{P_6B_S}{F_1} - P_7T_S\right] \Big/ P_8$$

$$\tilde{B}_{01} = F_1\tilde{B}_{0\alpha} + \frac{U_{1B}}{a_1}\tilde{B}_\alpha$$

$$\tilde{B}_1 = \frac{a_1}{U_{1B}}\left(F_{1S}^2 - F_1^2\right)\tilde{B}_{0\alpha} - F_1\tilde{B}_\alpha$$

$$\tilde{A}_1 = \left[4\zeta_1\sqrt{a_1}\,(a_1r_1-4)\tilde{B}_1 + 4\zeta_\alpha\sqrt{a_1r_1}\,a_1F_1\,\tilde{B}_\alpha\right]/P_1$$

$$\tilde{A}_\alpha = \left[4\zeta_\alpha\sqrt{a_1r_1}\,(a_1-4)\tilde{B}_\alpha + 4\zeta_1\sqrt{a_1}\,K_1a_1F_1\,\tilde{B}_1\right]/P_1$$

where

$$P_1 = (a_1-4)(a_1r_1-4) - K_1a_1^2F_1^2$$

$$P_2 = a_1\left[-P_1 + (4\zeta_1\sqrt{a_1})(4\zeta_\alpha\sqrt{a_1r_1})\right]$$

$$P_3 = (a_1-4)P_1 + (a_1r_1-4)(4\zeta_1\sqrt{a_1})^2$$

$$P_4 = (a_1r_1-4)P_1 + (a_1-4)(4\zeta_\alpha\sqrt{a_1r_1})^2$$

$$P_5 = F_1P_2 + 2U_{1B}^2P_1/a_1F_1$$

$$P_6 = -2U_{1B}P_1 + a_1(F_{1s}^2-F_1^2)P_3/U_{1B}$$

$$P_7 = -2U_{1B}P_1 + a_1(F_{1s}^2-F_1^2)P_2/U_{1B}$$

$$P_8 = P_6\left(\frac{P_4}{K_1F_1} - P_5\right) - P_7F_1(P_2-P_3)$$

$$F_{1s} = \sqrt{\pi_1/K_1}$$

(2.30)

The characteristics of this steady state solution is same as discussed in Chapter 2.3. The solution oscillates at the forcing frequency W_F. There is a constant center shift $\tilde{B}_{01}$ $\tilde{B}_{0\alpha}$. If the damping is sufficiently small infinite amplitude will appear over a finite frequency gap. Figure 20 shows the steady state response amplitude $V_T/\ell = 2\sqrt{\tilde{A}_1^2 + \tilde{B}_1^2}$ (since $h_1(1) = 2$) and $\theta_T = \sqrt{\tilde{A}_\alpha^2 + \tilde{B}_\alpha^2}$ where V_T and θ_T are bending and torsion tip amplitudes in inches and radians respectively, plotted against forcing frequency W_F for the damping case. The damping coefficients are obtained experimentally and has been shown in Figs. 10 and 11. Since they vary with amplitude, an iterative scheme is used to determine the final amplitude within 0.005 V_T/ℓ and 0.005 radians, accuracy. V_T/ℓ are of order 10^{-3} and has not been plotted. The constant terms in the assumed solution are of order 10^{-2}. Figure 20 also shows the experimental points. It is seen that the linear theory gives a fairly good estimate of the torsion amplitudes for W_F less than 17 CPS, considering that, the error involved in the forcing frequency measurement is of order 0.1 CPS. It may be noted that the sharp drop in torsion amplitude near $W_F \simeq 17$ CPS for all amplitudes of base motion is due to the fact that the upper instability boundary is independent of the base amplitude U_B (Fig. 5b).

CHAPTER 3

EXPERIMENTAL INVESTIGATION

3.1 Test Setup

The setup for the experimental observation of lateral vibration behavior of flexible beam under vertical excitation is shown in Figs. 1 and 2. The schematic sketch is given in Fig. 3. The test specimen chosen is a 0.02 in. thick 3.0 in. wide AL 6061-T6 beam, clamped at one end to form a 24.0 in. cantilever. The base is mounted rigidly to the shake-table such that the web of the beam is vertical. The shake-table oscillates vertically and generates a harmonic excitation over a frequency range from 2 to 50 CPS. The frequency of the shake-table is measured by using a strain gage mounted on a thin bar which is bolted to the shake-table at one end and fixed at the other.

The bending frequency and amplitude are derived from the signal from two strain gages mounted on each side of the beam near the root along the longitudinal principal axis. These strain gages do not respond to twisting about that axis, and form two arms of the balancing bridge. This eliminates temperature error. The torsion amplitude and frequency are derived from the four strain gages, two of which are mounted symmetrically at 45° about the longitudinal axis. The other two are placed alike directly on the other side of the beam.

They act as four arms of the bridge as shown in Fig. 3. The torsion strain gages pickup some signal when the beam is bending but this does not show up in the recordings when the twisting frequency is different from the bending frequency. The signal picked up by the torsion gage for pure static bending is shown in Fig. 7.

3.2 Test Procedure

The beam is clamped so that its web is vertical near the root with respect to the horizontal shake-table. It is observed that the beam because of its flexibility and initial imperfections leans slightly to the negative Y_o direction. The tip static deflection is estimated to be 0.25 inches. The bending and torsion response of the beam is investigated over the forcing frequency range from 2 to 30 CPS for four different base amplitudes of 0.0125, 0.025, 0.0375 and 0.050 inches. The strain gages are first calibrated for static deflection and twist due to a point load and torque at the tip. The strain gages are then calibrated dynamically by exciting the beam at different measurable tip amplitudes in first, second, and third bending mode and in first twisting mode. These are shown in Figs. 8 and 9. The static calibration which could be done only for first bending and first torsion are also shown after zero correction. Only the dynamic calibration is used for conversion.

To estimate the damping ratio, dynamic decay record is taken for first and second bending and first torsion. Some

typical records are shown in Figs. 12 and 13. The torsion channel of Fig. 12 shows how the torsion gages picks up bending. From bending channel of Fig. 13, it is apparent that the bending gages do not pickup appreciable torsion. The damping ratios are determined from the slope of the decay records plotted on sami-log papers. The variations of damping ratio with amplitude are shown in Figs. 10 and 11.

For a particular run with U_{1B}, ζ_1, ζ_2, ζ_α already determined, only the parameter a_1 was varied by varying the forcing frequency W_F of the system. The forcing frequency was increased (and decreased) in a stepwise manner until the necessary regions of interest were covered. Occasionally the beam is disturbed or released from the rest to determine the stability and the limit cycle type behavior. Some records of the response at the three regions of instability are shown in Figs. 14, 15, and 16.

3.3 Discussion of Experimental Results

The overall picture of amplitude response over a frequency range up to W_F = 30 CPS is shown in Fig. 17. V_T/ℓ represents the ratio of tip bending amplitude to beam length. θ_T in the tip twist in radians. The dynamic calibration charts corresponding to the predominant mode shape is used for conversion from the recording to V_T/ℓ and θ_T. The experimentally measured natural frequencies of the beam were

first bending mode - 1.08 CPS

second bending mode - 7.00 CPS

first torsion mode - 17.00 CPS.

For W_F from 2 to 7 CPS there is no appreciable response. At 7 CPS a mild second bending mode is obtained. Even though the second instability region at second bending is extremely narrow it is excited by the forcing function in the right hand side of Eq. (2.18b) due to initial static deflection. For W_F from 7 to 14 CPS there is no appreciable response.

Between W_F = 14 to 30 CPS there are three principal regions of interest. The first of these regions is at $W_F \simeq 17$ CPS and has been shown in an enlarged scale in Fig. 18. As W_F approaches 17 CPS the torsion amplitude becomes larger. The bending is negligibly small and the torsion is in the first torsion mode at the forcing frequency. Then at W_F little below 17 CPS depending on the amplitude of the base motion, the beam suddenly leans to the side in which it had a initial static deflection, then executes an irregular whipping motion on either side. This occurs for 0.0375 in. and higher base amplitudes and is termed as snapping here. For 0.0125 in. and 0.025 in. base amplitudes, as W_F crosses 17 CPS, the torsion amplitude reaches a peak; the beam snaps mildly then dies down to no torsion and bending. A sample record of steady state torsion is shown in Fig. 14.

The amplitude response near the second region of interest near W_F = 18.4 CPS is also plotted in Fig. 18. The steady amplitude values are connected by dotted lines. The scattered points show an estimated mean of the unsteady amplitude values.

Here the beam exhibits limit cycle type behavior for small base amplitudes. For 0.0125 and 0.025 in. base amplitudes, initially there is very small vibration near $W_F \simeq 18.4$ CPS. When given a light kick the oscillations die down. With a large kick, the beam falls into a steady bending oscillation in first mode at little below 1 CPS with small ripples at W_F superimposed on it and undergoes torsion at little above 17 CPS. A sample record of this phenomenon is shown in Figs. 15a and 15b for 0.0125 in. base amplitude. For this case the torsion amplitude is also steady. It may be noted that the undulations in the torsion channel record of Figs. 15a, b are due to the torsion channel picking up a fraction of bending at the bending frequency. Fig. 15c shows the same phenomenon for 0.025 in. base amplitude. Here the superimposed W_F on bending response is pronounced and the torsion amplitude is somewhat unsteady. At higher base amplitudes the response becomes more unsteady and at 0.05 in. base amplitude the beam snaps by itself in this region when released from rest. Two sample response records are shown in Fig. 15d and 15e for 0.0375 in. and 0.05 in. base amplitudes respectively.

Between the two regions at $W_F \simeq 17$ and 18 CPS discussed above, there is a quiet region at lower base amplitudes. At base amplitude 0.05 in. and above the two instability regions merge. The beam snaps by itself at $W_F \simeq 16.4$ CPS and does not become stable again until W_F reaches 21.0 CPS. At $W_F \simeq 19$ CPS a mild third bending mode is obtained because the natural

frequency of the third bending mode is about 19 CPS.

The region between W_F = 19 CPS to 22 CPS is relatively quiet. Then another instability region is encountered where the beam oscillates predominantly in the second bending mode and twists in the first torsion mode. The amplitude response is shown in Fig. 19 with the bending amplitude in an enlarged scale. As W_F approaches 24 CPS, the second bending and first torsion amplitudes grow and at a certain frequency they are bigger for larger base amplitudes. The beam is stable and goes back to the same state when disturbed. The bending frequency is about 7 CPS and goes down to 6 CPS at higher amplitudes. A sample record is shown in Fig. 16a. The amplitudes reach a peak near $W_F \simeq 24$ CPS. Here the bending frequency is about 6 CPS and torsion frequency, about 18 CPS. The beam executes a large flapping motion. The amplitudes vary somewhat irregularly. A sample record at 0.0125 in. base amplitude is shown in Fig. 16b. The beam is released from the rest and the response is recorded at slow speed. The amplitudes of vibration grow to a certain amplitude, then becomes more or less steady. The later portion is recorded at high speed to reveal the wave form. At higher base amplitudes the motion becomes more irregular. Two sample response records at large attenuation are shown in Fig. 16c and 16d, for 0.025 in. and 0.0375 in. base amplitude. The later record shows a beating phenomena near W_F = 23.3 CPS. These responses are basically nonlinear in nature. Behaviors become nonlinear for tip deflections

of 1 in. or more.

As W_F exceeds 25 CPS the beam quiets down for 0.0125 in. base amplitude. For 0.025 and 0.0375 in. base amplitude the motion becomes relatively small as W_F approaches 26 CPS. Beyond this the beam still vibrates in second bending mode at about 7 CPS and twists irregularly at high frequencies but the amplitudes are small. Beyond W_F = 30 CPS the amplitudes rise sharply indicating another instability region but this was not investigated here.

A concise summary of the typical response behavior of the beam is presented in Table 2 for each of the four base amplitude motions tested.

CHAPTER 4

CONCLUSIONS

The present report has investigated the dynamics of lateral bending and torsion vibration of a thin flexible beam under vertical harmonic excitation, both theoretically and experimentally. Only the linear equations are considered for the theoretical analysis.

The governing equations for an initially straight beam for small motion are two coupled homogeneous equations representing lateral bending and torsion dynamic equilibrium. Since the experimental specimen had a static deflection due to built-in imperfection, inclusion of this gives rise to forcing terms on the right hand side of the homogeneous equations. Using Galerkin's method with assumed normal modes one gets as many equations as number of mode shapes assumed. These are to be analyzed in time domain. The homogeneous part of the equations have the same characteristics as the Mathieu equation[1]. Because of the forcing terms on the right hand side, parametric and forced excitation coexist and the main interactions occur near the second instability region of Strutt's diagram. These coupled linear equations are complex enough to forbid one from writing down the approximate closed form general solutions as usually done for a one degree of freedom system, but the procedure for obtaining solutions has been outlined. The first and second instability regions for no

damping has been determined and the steady state solutions computed. They have the well known characteristics of having infinite amplitude response over a finite range of forcing frequencies. In the second instability region only the region near the torsion natural frequency is significant and is encountered in the experiment. Mild presence of other regions are also observed.

Experimentally, the beam was excited at four different base amplitudes over a forcing frequency range up to 30 CPS. Essentially, instabilities at three frequency regions have been obtained; whose characteristics can be clearly observed at low base amplitudes. At W_F near 17 CPS the beam twists at the forcing frequency and has negligible bending amplitude until the beam snaps. This is a linear phenomena and the experimental results compare reasonably well with the theoretical solution. The beam has another instability region around $W_F \simeq 18.4$ CPS and exhibits limit cycle type behavior at low base amplitudes, with the beam oscillating at 1 CPS and twisting at 17 CPS. This is essentially a nonlinear phenomena and cannot be explained by linear theory. Another instability region is obtained near $W_F \simeq 24$ CPS in which bending is predominantly in the second bending mode vibrating at about 6 CPS and the torsion is in the first torsion mode twisting at about 18 CPS. When released from rest the amplitudes grow until they settle into a limit cycle. These are all nonlinear characteristics since the linear theory will give solutions where the response

frequency can only be $\frac{W_F}{2}$, $\frac{3}{2}$ W_F..;W_F, $2W_F$.... etc., and cannot give any limit cycle. Thus one has to go into the nonlinear formulation of this problem to predict such behaviors. The response becomes nonlinear for tip deflection of 1 in. or more. The nonlinear terms are not quite well defined and one gets different equations proceeding in different manners.

For future work one may look at the nonlinear problem and try to explain the experimental results which are presented in detail. Bolotin[1] has briefly discussed the nonlinear problem but the solution is inadequate to explain the nonlinear behaviors observed. Thus in working with similar structural configuration and loading one has to carry out a careful experimental investigation without relying entirely on the theoretical linear analysis.

APPENDIX A

MODE SHAPES

The mode shapes in bending and torsion are chosen so as to satisfy the dynamic equilibrium in free vibration and the associated boundary conditions[4]. They are

$$h_K(\eta) = \cosh \lambda_K \eta - \cos \lambda_K \eta - \sigma_K (\sinh \lambda_K \eta - \sin \lambda_K \eta)$$

$$\alpha_K(\eta) = \sin \Omega_K \eta$$

where K refers to the mode shape.

$$\Omega_K = (2K-1)\pi/2$$

λ_K and σ_K are tabulated in Ref. 4 part of which is reproduced below.

MODE	σ_K	λ_K	λ_K^4
1	0.73410	1.8751	12.362
2	1.01847	4.6941	485.52
3	0.99923	7.8548	3806.5
4	1.000043	10.9955	14617.0

APPENDIX B

EVALUATION OF CONSTANT TERMS

$$A_1 = \int_0^1 (h_1)^2 d\eta = 1 \qquad A_2 = \int_0^1 (h_2)^2 d\eta = 1$$

$$B_1 = \int_0^1 (h_1'')^2 d\eta = 12.362 \qquad B_2 = \int_0^1 (h_2'')^2 d\eta = 485.52$$

$$C_1 = \int_0^1 (1-\eta)^2 \alpha\, h_1'' d\eta = 0.4206 \qquad C_2 = \int_0^1 (1-\eta)^2 \alpha\, h_2'' d\eta = -1.6361$$

$$D = \int_0^1 (\alpha)^2 d\eta = 0.500 \qquad [\ \alpha \text{ DENOTES } \alpha_1\ ]$$

$$H = \int_0^1 (\alpha')^2 d\eta = 1.2337$$

$$C_{S1} = \int_0^1 (1-\eta)^2 \theta_S\, h_1'' d\eta$$

$$C_{S2} = \int_0^1 (1-\eta)^2 \theta_S\, h_2'' d\eta$$

$$S = \int_0^1 (1-\eta)^2 h_S''\, \alpha\, d\eta$$

(B.1)

The constants C_{S1}, C_{S2}, and S are evaluated by assuming that the built-in deflection and twist h_B, θ_B and static deflection and twist h_S, θ_S are similar to the assumed first

bending and torsion mode shapes respectively and differ only in amplitudes.

So we write

$$\theta_B = T_B \alpha(\eta) \qquad \theta_S = T_S \alpha(\eta)$$
$$\frac{V_B}{\ell} = B_B h_1(\eta) \qquad \frac{V_S}{\ell} = B_S h_1(\eta) \tag{B.2}$$

where T_B, B_B, T_S, B_S are constants.

Thus we have

$$C_{S1} = T_S C_1$$
$$C_{S2} = T_S C_2 \tag{B.2a}$$
$$S = B_S C_1$$

and one needs to evaluate only T_S and B_S. Since Eq. (B.2) must satisfy static equilibrium Eqs. (2.8), (2.9), we introduce them and apply Galerkin's technique using $h_1(\eta)$ and $\alpha(\eta)$ as the weighing functions respectively, to get

$$\frac{EI}{\ell^4}\left[(B_S - B_B)B_1\right] - \frac{mg}{2\ell} T_S C_1 = 0 \tag{B.3}$$

$$-\frac{GJ}{\ell^2}\left[(T_S - T_B)H\right] + \frac{mg\ell}{2} B_S C_1 = 0 \tag{B.4}$$

using the definitions in Eq. (B.1). After slight manipulation and using the notations introduced in Eq. (2.15) they reduce to

$$(B_S - B_B) - F_1 T_S = 0 \qquad (B.5)$$

$$(T_S - T_B) - \frac{F_1 K_1}{r_1} B_S = 0 \qquad (B.6)$$

Solving for B_S and T_S

$$B_S = (B_B + T_B F_1) \Big/ \left(1 - \frac{F_1^2}{F_{1S}^2}\right) \qquad (B.7)$$

$$T_S = \left(T_B + \frac{F_1}{F_{1S}^2} B_B\right) \Big/ \left(1 - \frac{F_1^2}{F_{1S}^2}\right) \qquad (B.8)$$

where $F_{1S} = \sqrt{r_1/K_1}$

For our specimen there is no appreciable built in twist but V_S is estimated to be 0.25 inches in negative Y_o direction. Thus one need not measure B_B and has

$$B_s = -0.25/2\ell = -0.00521$$

SINCE $h_1(1) = 2$, $T_B = 0$

$$T_s = \frac{F_1}{F_{1S}^2} B_S = -0.00237$$

Thus from Eq. (B.2a)

$$C_{s1} = -0.00237\, C_1$$

$$C_{s2} = -0.00237\, C_2$$

$$S = -0.00521\, C_1$$

It may be noted from Eqs. (B.7), (B.8) that the static buckling will occur when $F_1 = F_{1S}$ with the natural free vibration mode assumption. For the experimental specimen $F_1 = 0.0735$ and $F_{1S} = 0.4016$.

REFERENCES

1. Bolotin, V.V., Dynamic Stability of Elastic Systems, Holden-Day Inc., San Francisco, California, 1964.

2. Chhatpar, C.K. and Dugundji, J., Dynamic Stability of Pendulum Under Parametric Excitation, M.I.T. Aeroelastic and Structures Research Laboratory, Report TR 134-4, AFOSR-69-0019TR, December 1968.

3. Chhatpar, C.K. and Dugundji, J., Dynamic Stability of Pendulum Under Coexistence of Parametric and Forced Excitation, M.I.T. ASRL Report TR 134-5, AFOSR-68-0001, December 1967.

4. Young, D., Vibration of Rectangular Plates by Ritz Method, Journal of Applied Mechanics, 17, 4, pp. 448-453, 1950.

TABLE 1

BEAM PARAMETERS

Length	ℓ = 24.0 in.
Width	d = 3.0 in.
Thickness	b = 0.02 in.
Material	= AL 6061-T6
Density	ρ = 0.000253 lb-sec^2/in.^{4}
Modulus of Elasticity	E = 10^7 psi
Poisson's Ratio	ν = 0.3

First bending mode natural frequency

W_{1h} = 1.08 CPS (Theory 1.115 CPS)

Second bending mode natural frequency

W_{2h} = 7.00 CPS (Theory 6.988 CPS)

First torsion mode natural frequency

W_α = 17.0 CPS (Theory 17.12 CPS)

$m = \rho bd = 0.1518 \times 10^{-4}$ lb-sec^2/in^2

$I_m = \frac{m}{12}(b^2+d^2) = 0.1139 \times 10^{-4}$ lb-sec^2

$I = \frac{1}{12} db^3 = 2.0 \times 10^{-6}$ in^4

$J = \frac{1}{3} db^3 = 8.0 \times 10^{-6}$ in^4

TABLE 2

TYPICAL RESPONSE

BASE AMPLITUDE 0.0125 IN.

W_F†	BENDING MOTION††	TORSION MOTION+
16.2	Negligible	Small, Steady W=16.2
17.1*	Small, w=17.1	Moderate, Steady W=17.1
17.2	Negligible	Small, Steady W=17.2
18.4*	Moderate Steady in 1BM. W=1.0 Given small kick-decays Given big kick-above response	Large, Steady W=17.3
19.0	Small W=19.0	Negligible
23.4*	Moderate, Steady in 2BM. W=6.3	Moderate, Steady W=17.0
24.0	Large, Steady in 2BM. W=6.0	Large, Little unsteady W=18.0
24.6*	Large, Steady in 2BM. W=6.3 Released from rest-grows to above.	Large, Little unsteady W=18.0
2.50	Negligible	Small, Steady W=25.0

† All W and W_F are in cycles per second.

†† 1BM = 1st Bending Mode; 2BM = 2nd Bending Mode

+ Always in 1st Torsion Mode.

* Records shown in figures.

TABLE 2 (CONTINUED)

BASE AMPLITUDE 0.025 IN.

W_F†	BENDING MOTION††	TORSION MOTION+
15.0	Negligible	Small, Steady W=15.0
17.0	Negligible	Moderate, Steady W=17.2
17.4	Negligible	Small, Steady W=17.4
18.5*	Moderate, Steady in 1BM W=0.9 with 18 CPS superimposed. Given small kick-decays Given big kick-above response.	Large, Unsteady, Varying amplitude. W~17.5
20.0	Small, Steady W=20.0	Small, Steady W=20.0
23.0	Moderate, Steady in 2BM. W=6.2	Moderate, Steady. W=17.0
24.0*	Large, Irregular in 2BM. W=7.0	Large, Irregular. W=18.0
25.5	Large Irregular in 2BM. W=7.0	Large, Irregular. W=18.0
27.2	Moderate, in 3BM, W=19.0 Given small kick-in 2BM. W~7.0	Moderate, Irregular Many harmonics present.

TABLE 2 (CONTINUED)

BASE AMPLITUDE 0.0375 IN.

W_F †	BENDING MOTION††	TORSION MOTION+
7.0	Small, Steady in 2BM W=7.0	Negligible
16.8	Small, Steady in 1BM W=16.8	Moderate, Steady W=16.8
17.0	Snap by itself	Snap by itself
18.0	Moderate, Steady in 1BM W=0.9 with 18 CPS superimposed Lightly kicked, snap	Large, Unsteady, Varying amplitude W=17.0
18.4	Snap by itself	Snap by itself
19.3*	Large, Irregular in 1BM Initially-none. Lightly kicked-above response	Large, Irregular W≈17.0
21.0	Small in 3BM. W=19.0	Small, W=21 and 86
23.3*	Large, Beating type in 2BM. W≈6.0	Large, Beating type W≈18.0
24.4	Large, Irregular in 2BM W≈6.0	Large, Irregular W≈17.0
27.0	Moderate, Irregular in 2BM. W≈7.0	Large, Irregular, Many harmonics present

TABLE 2 (CONCLUDED)

BASE AMPLITUDE 0.050 IN.

W_F†	BENDING MOTION††	TORSION MOTION†
7.0	Small, Steady in 2BM W=7	Negligible
16.4	Negligible. Sway to one side. Given kick-snap	Large, Steady W=16.4
17.0	Snap by itself	Snap by itself
17.5	Initially none. Given small kick-snap	Large, Unsteady W≃17.0
18.7*	Released from rest- Amplitude grows slowly to snap	Torsion frequency 17.0 before snapping
21.0	Small, Steady in 3BM W=19. Kicked-snap, eventually comes back to above	Moderate Unsteady W=21 and 86
23.0	Large, Irregular in 2BM W≃6.0	Large Irregular W≃17.0
25.4	Large, Irregular flapping in 2BM. W≃6.0 Released from rest- grows to above	Large, Irregular
29.0	Small, Irregular in 2BM. W≃7.5	Large, Irregular

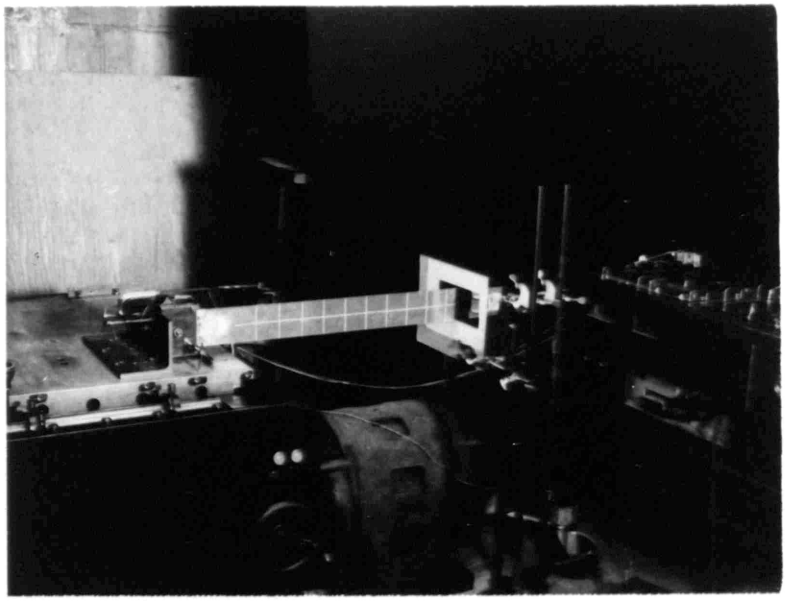

FIG. 1 OVERALL VIEW OF TEST SET UP

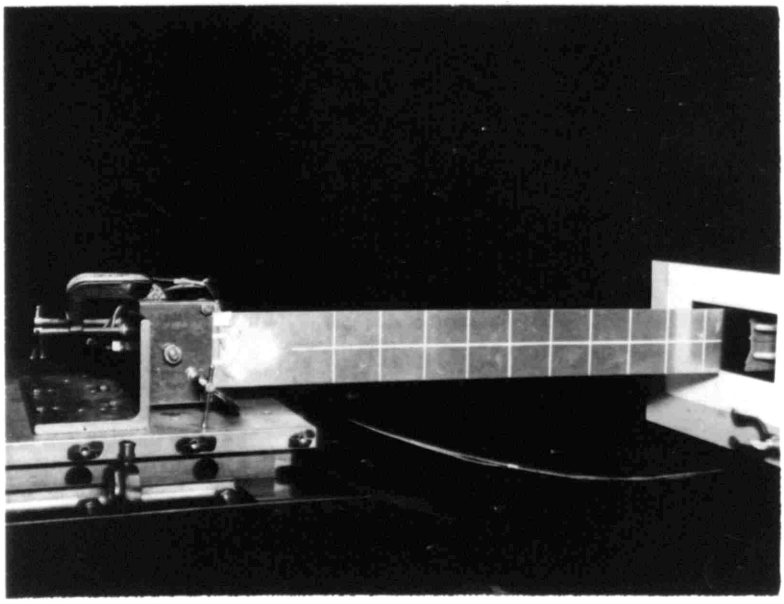

FIG. 2 CLOSE UP VIEW OF TEST SET UP

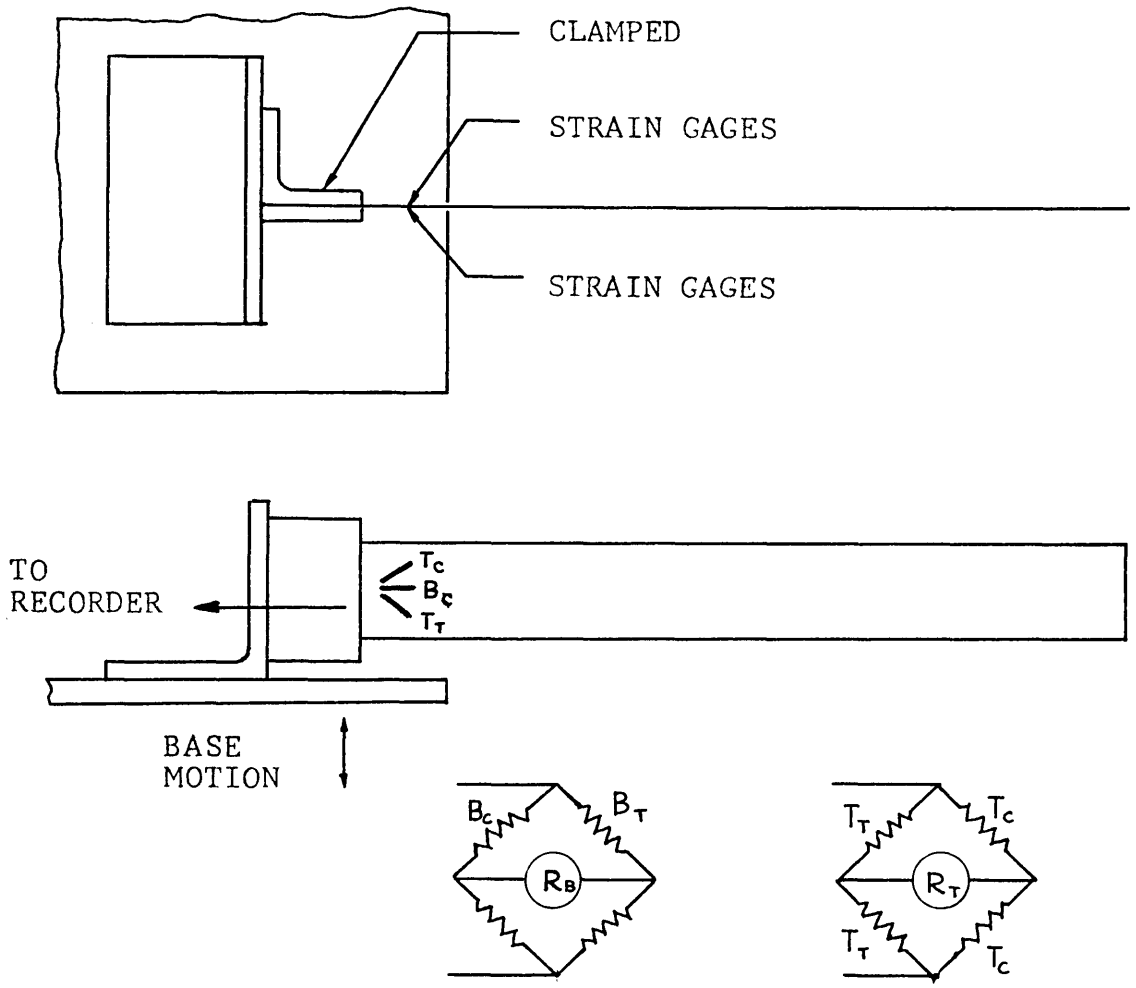

FIG. 3 SCHEMATIC DIAGRAM

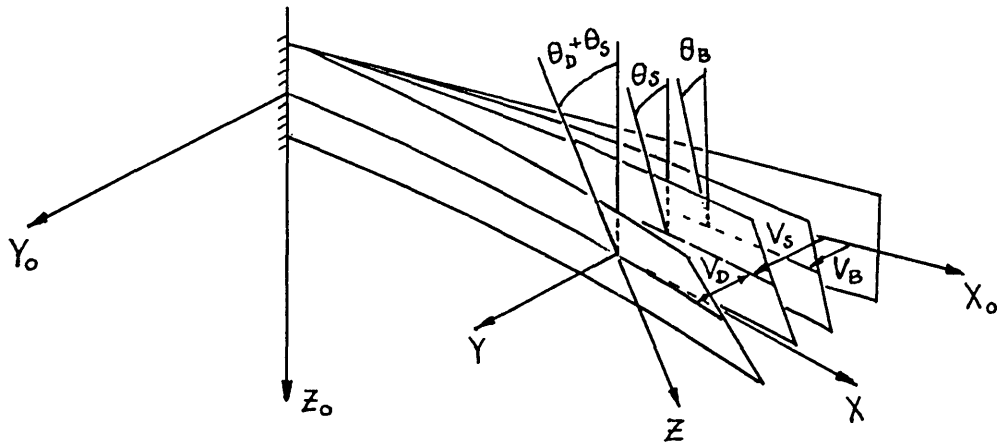

FIG. 4 COORDINATE SYSTEM

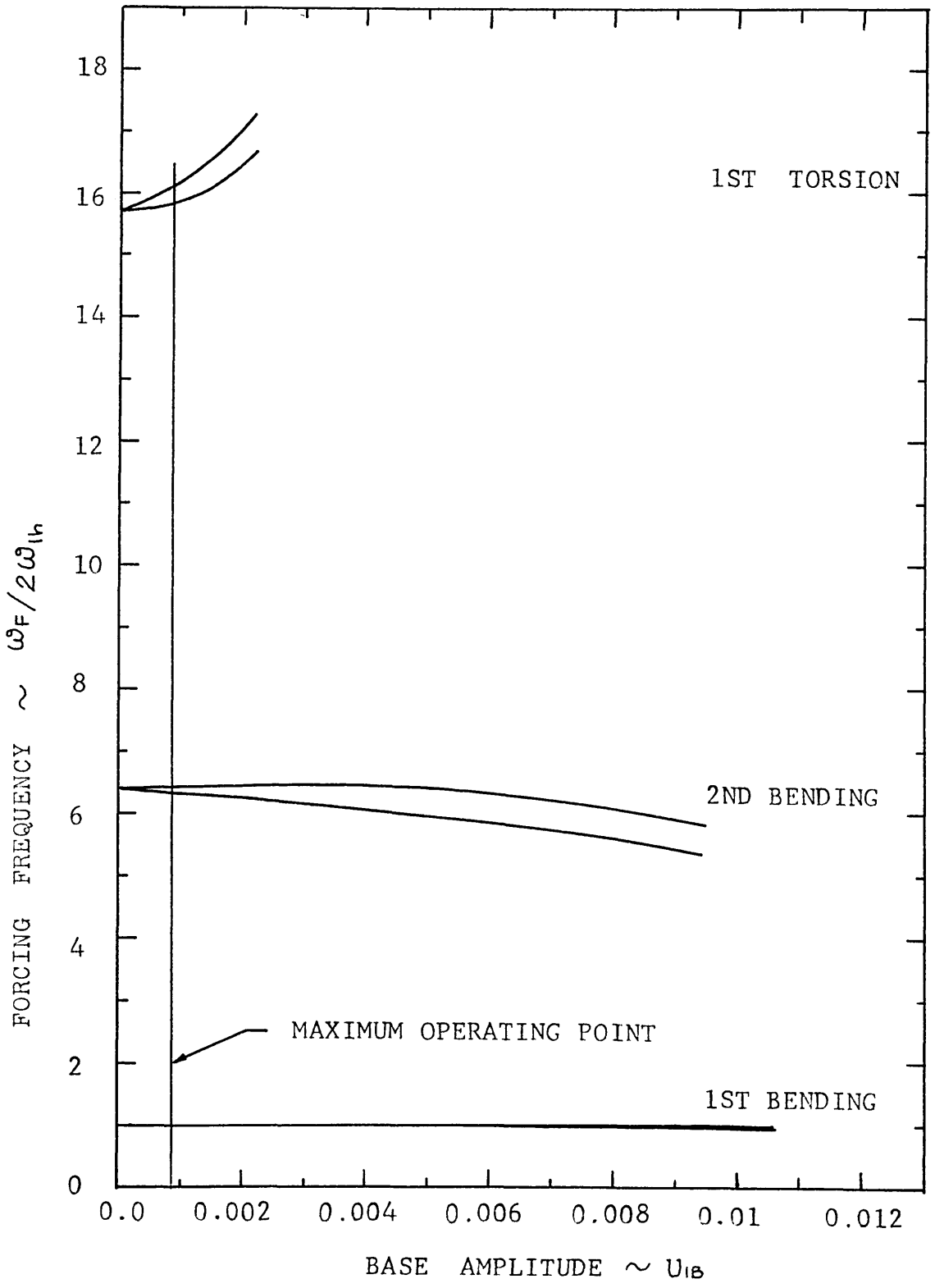

FIG. 5a FIRST INSTABILITY REGION

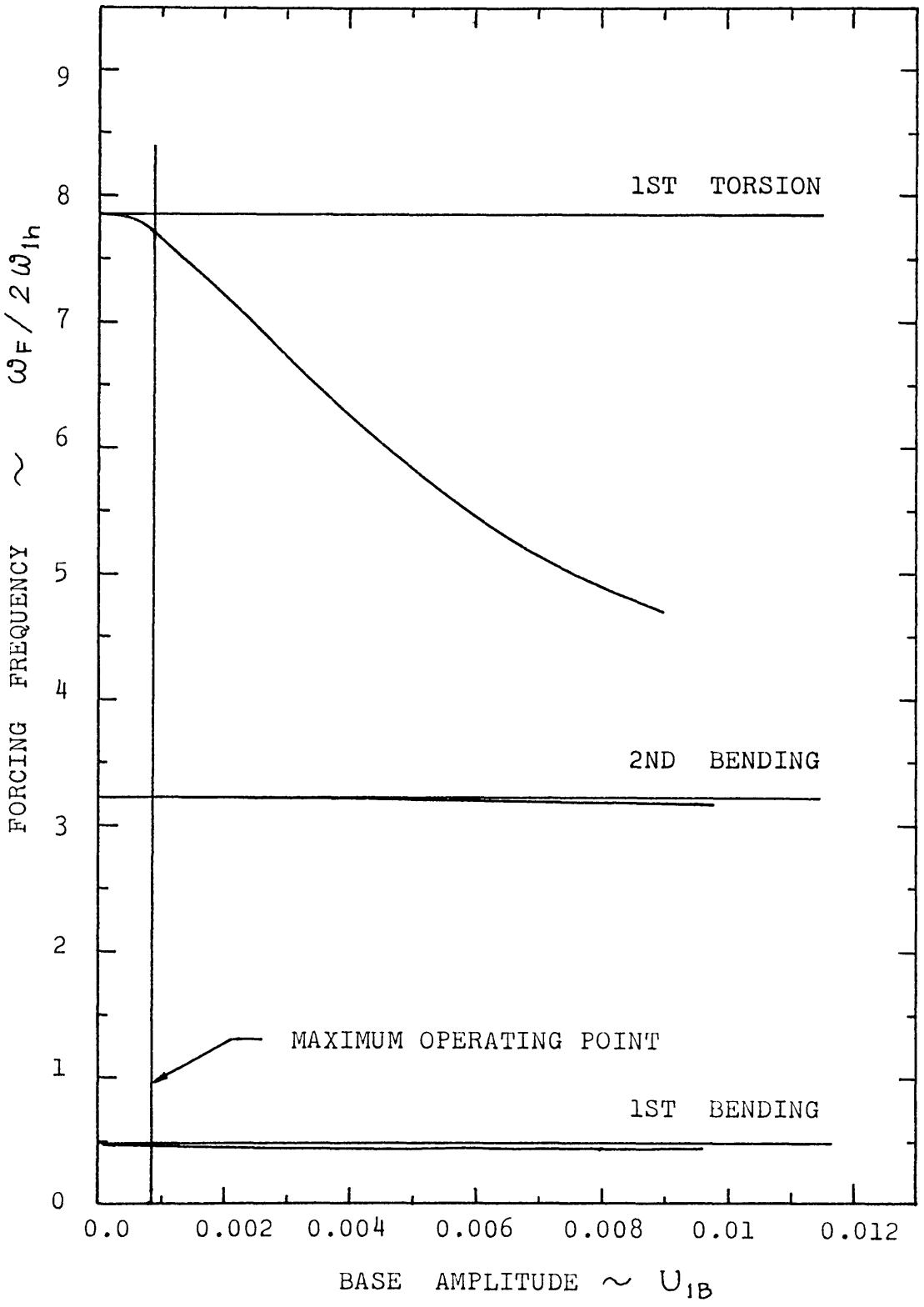

FIG. 5b SECOND INSTABILITY REGION

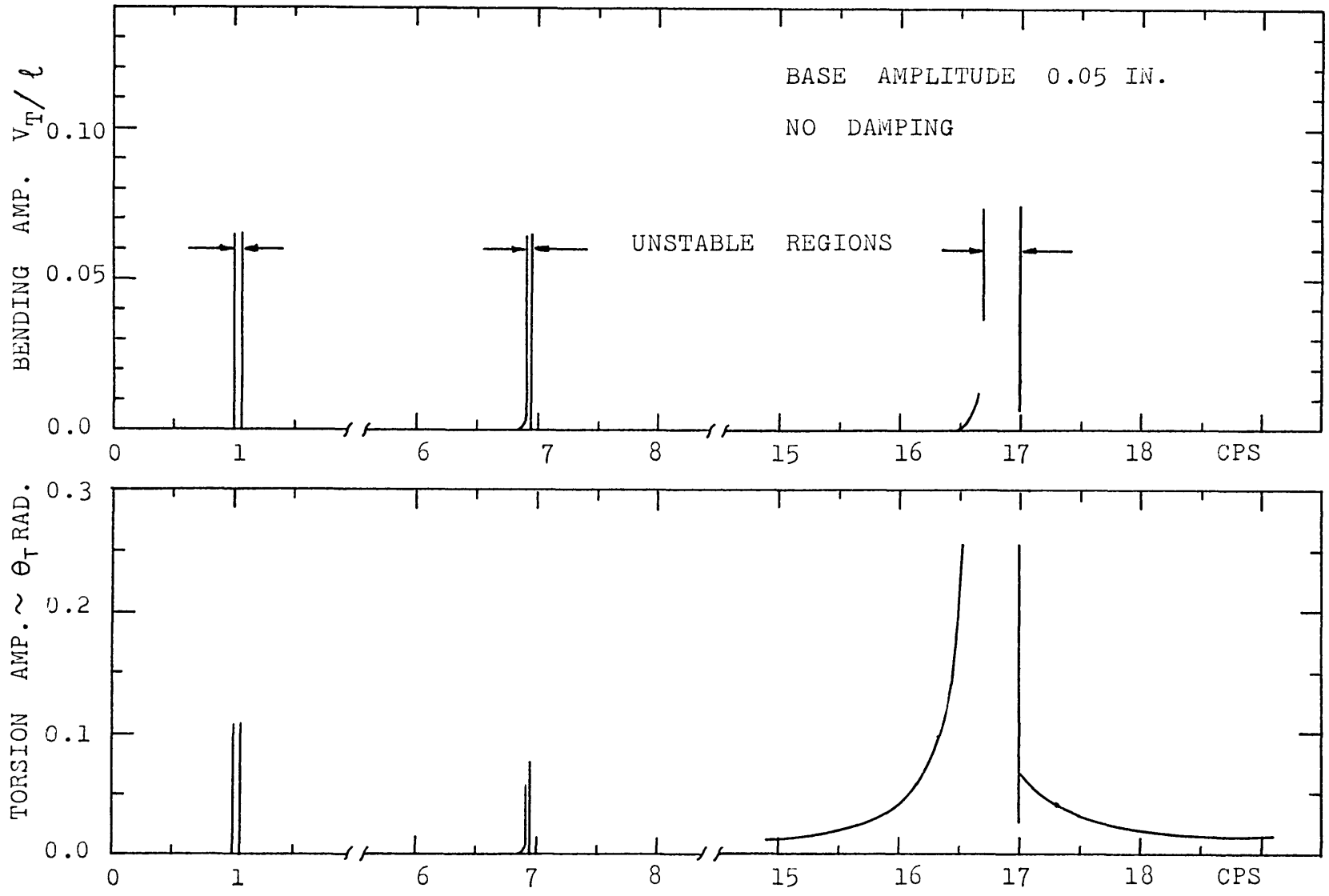

FIG. 5c THEORETICAL STEADY STATE AMPLITUDE VS. $W_F \sim$ CPS

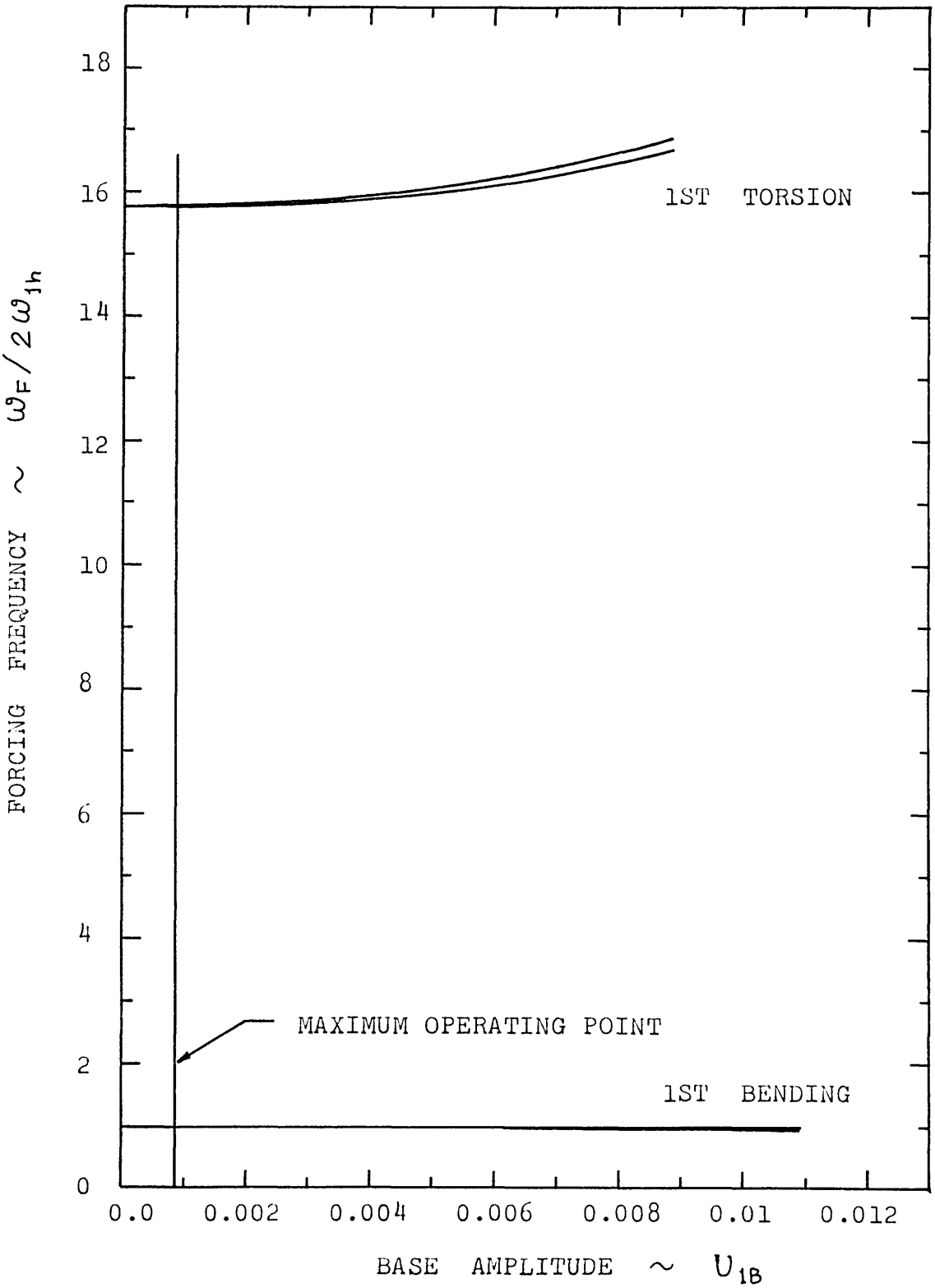

FIG. 6a FIRST INSTABILITY REGION

(TWO MODE APPROXIMATION)

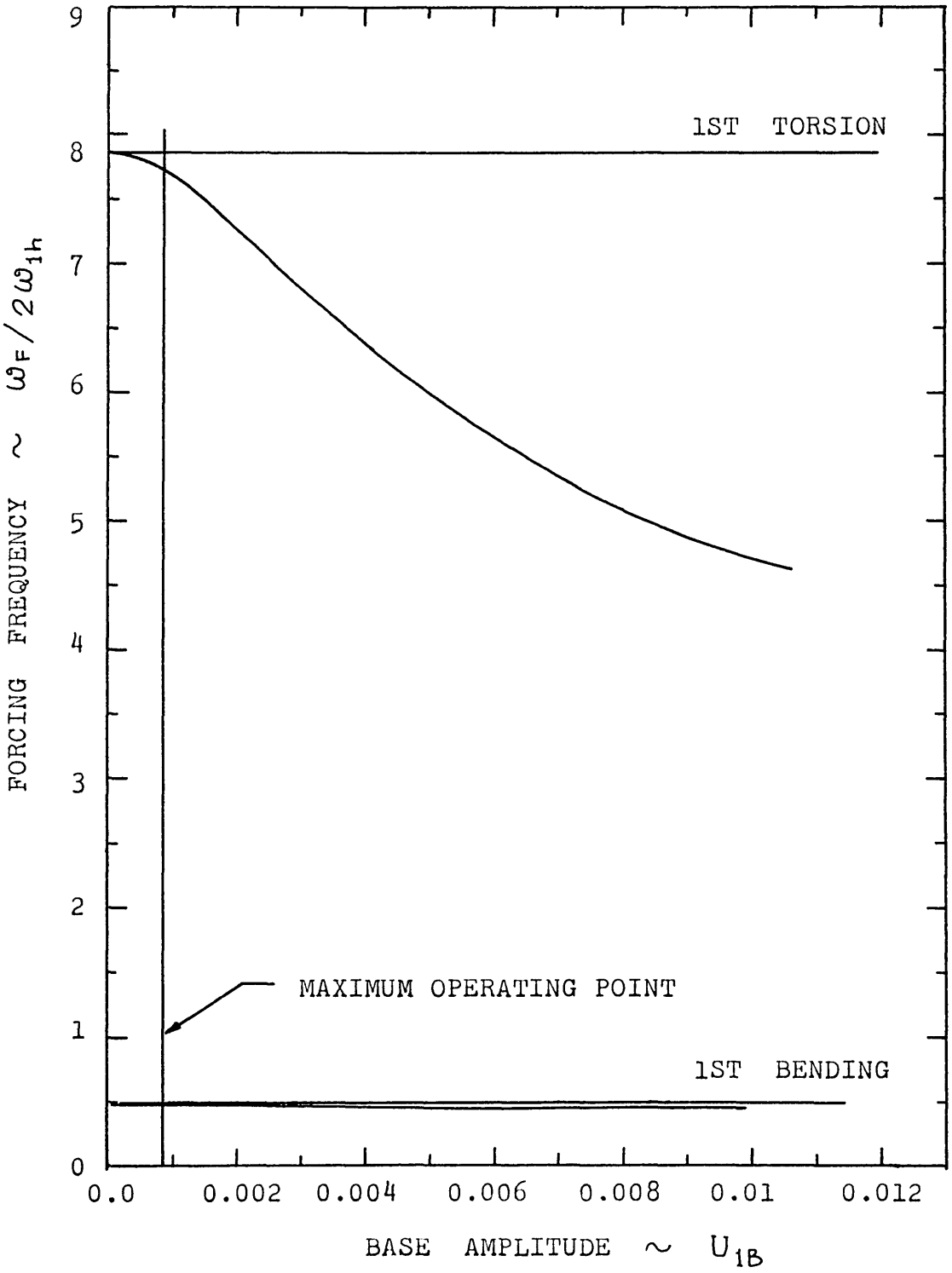

FIG. 6b SECOND INSTABILITY REGION

(TWO MODE APPROXIMATION)

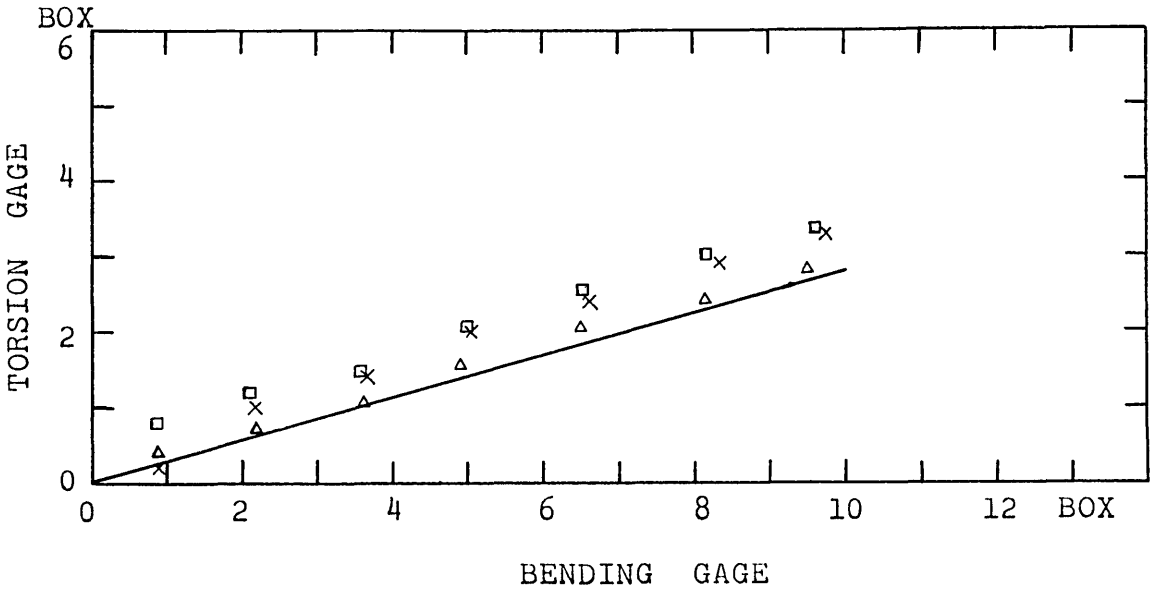

FIG. 7 READING IN TORSION GAGE FOR PURE STATIC BENDING

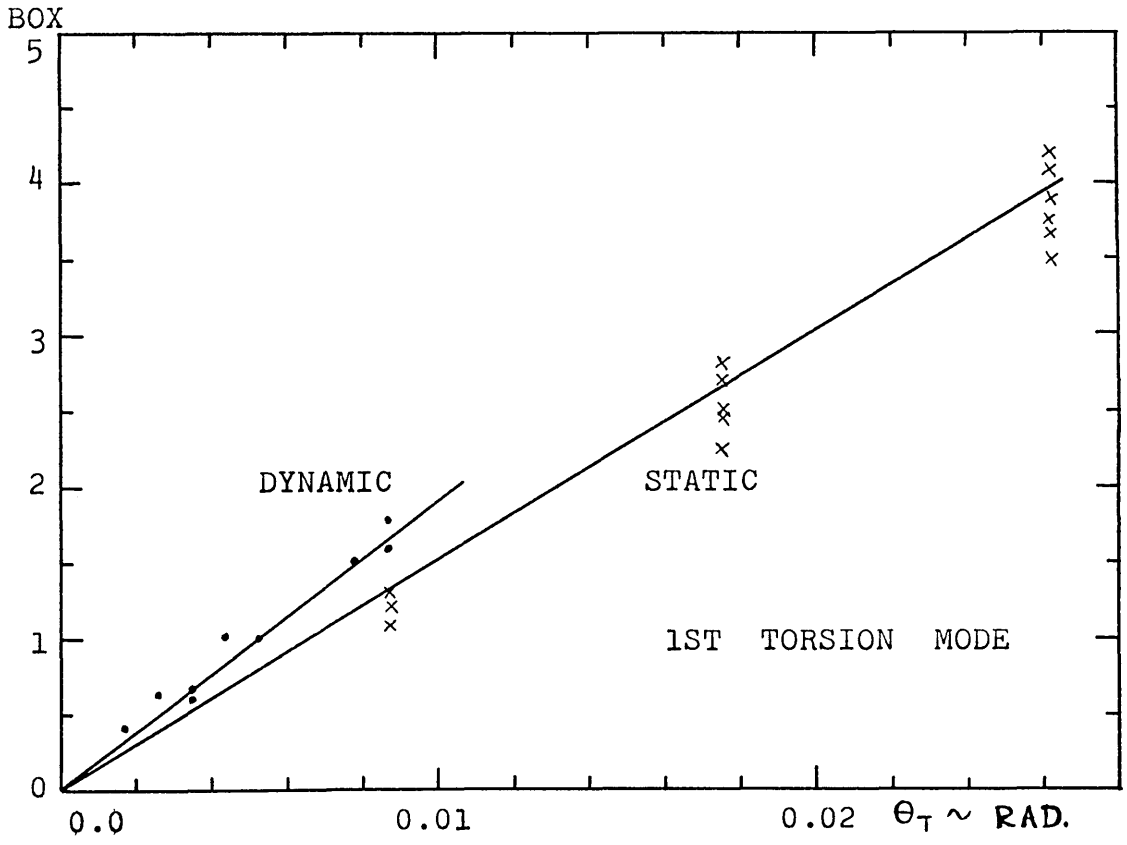

FIG. 8 TORSION GAGE CALIBRATION CHART

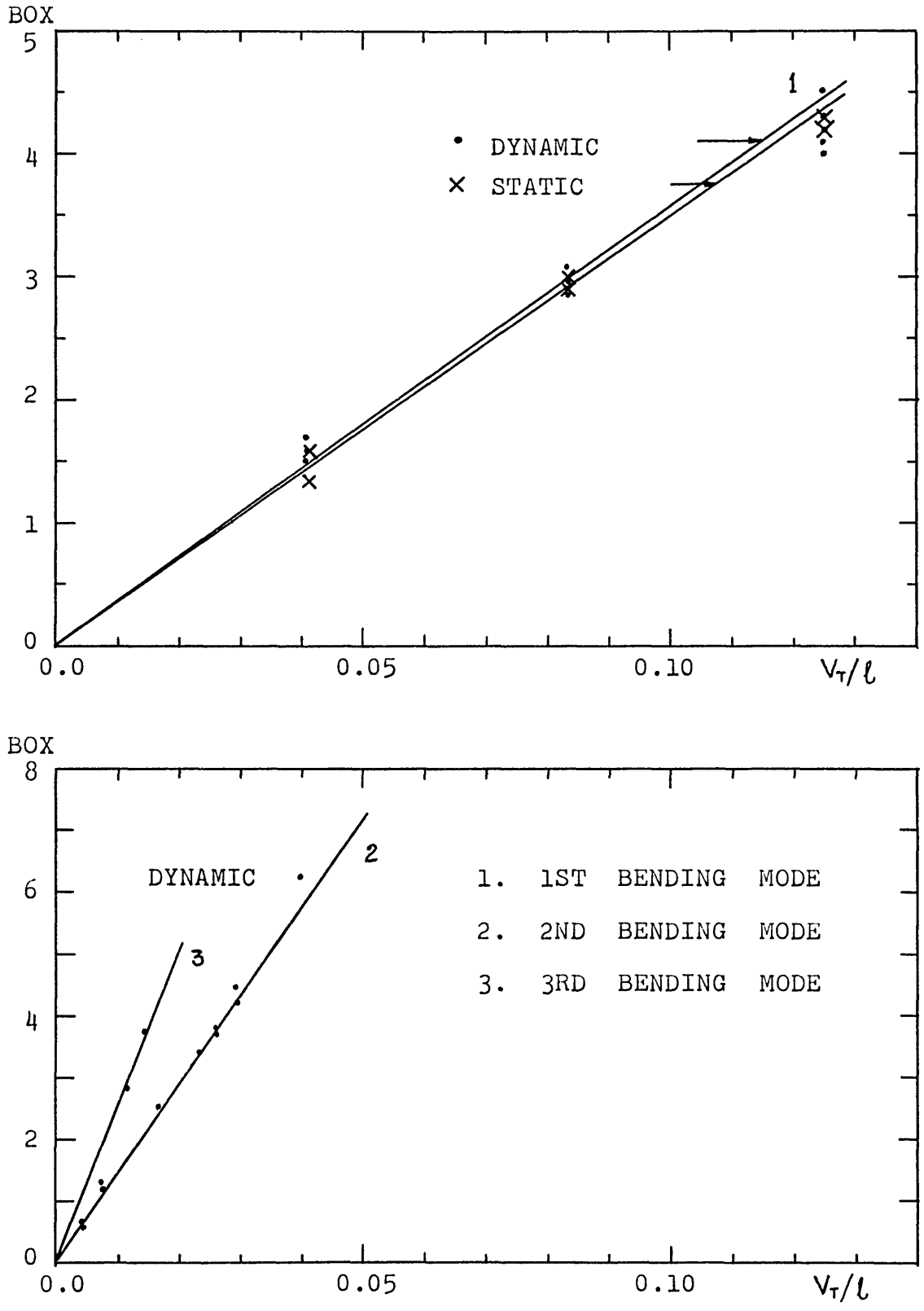

FIG. 9 BENDING GAGE CALIBRATION CHART

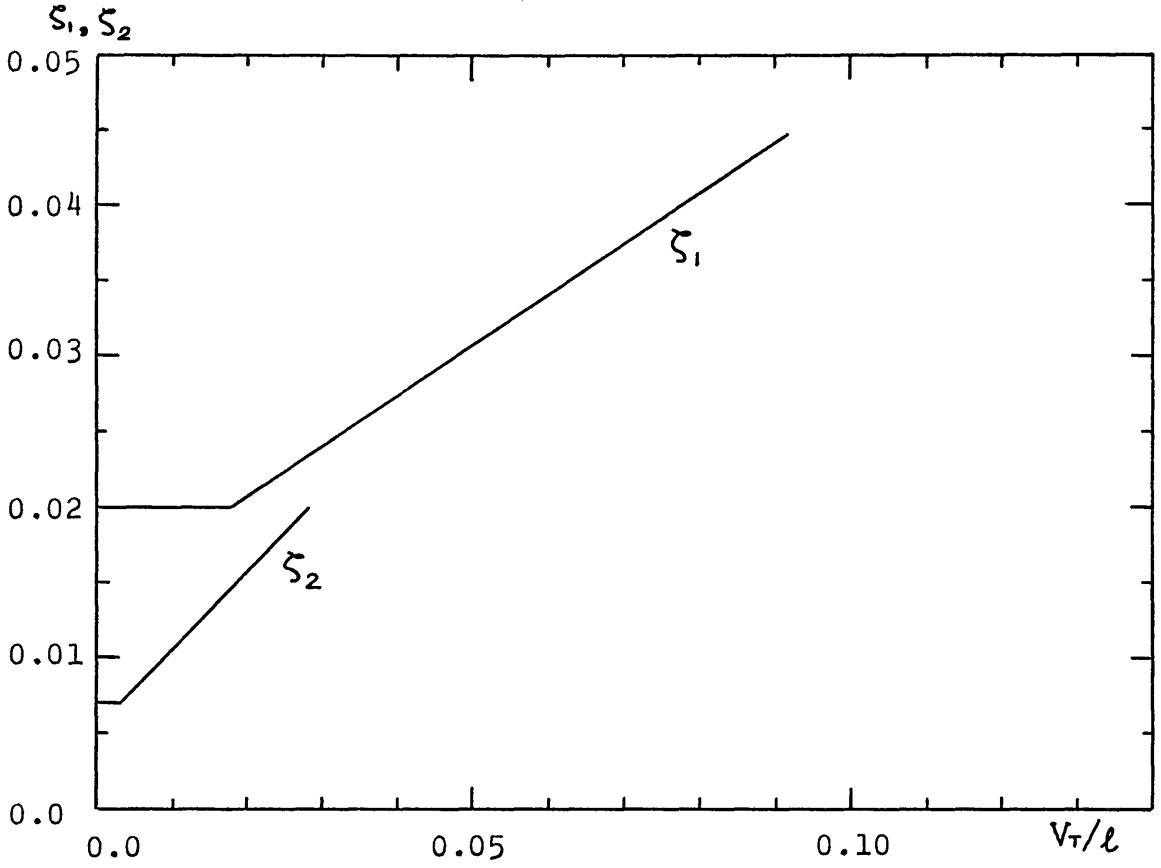

FIG. 10 DAMPING RATIO IN 1ST AND 2ND BENDING MODE

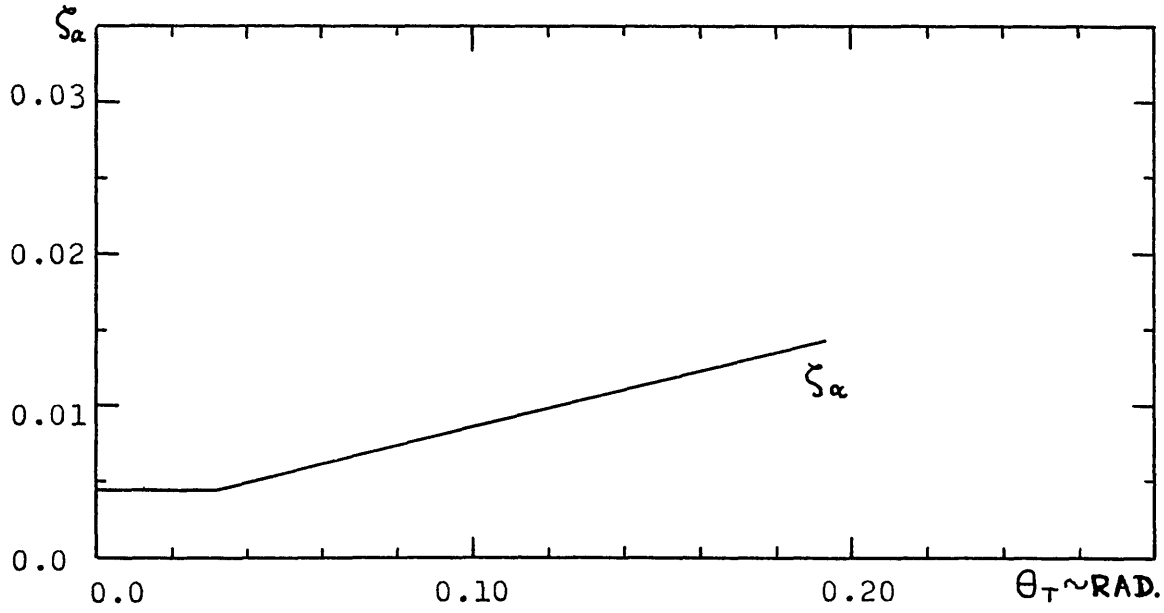

FIG. 11 DAMPING RATIO IN 1ST TORSION MODE

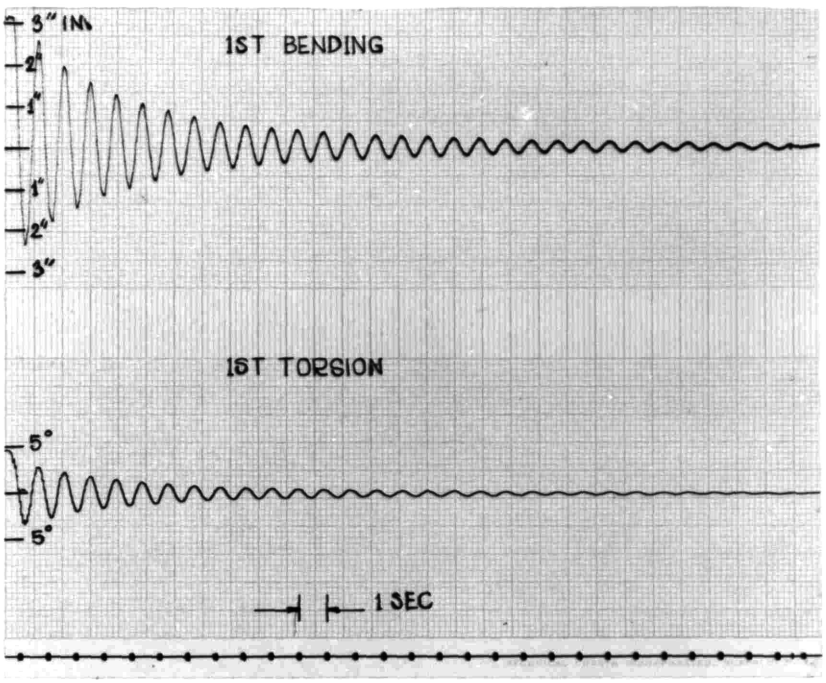

FIG. 12 SAMPLE FIRST BENDING DECAY RECORD

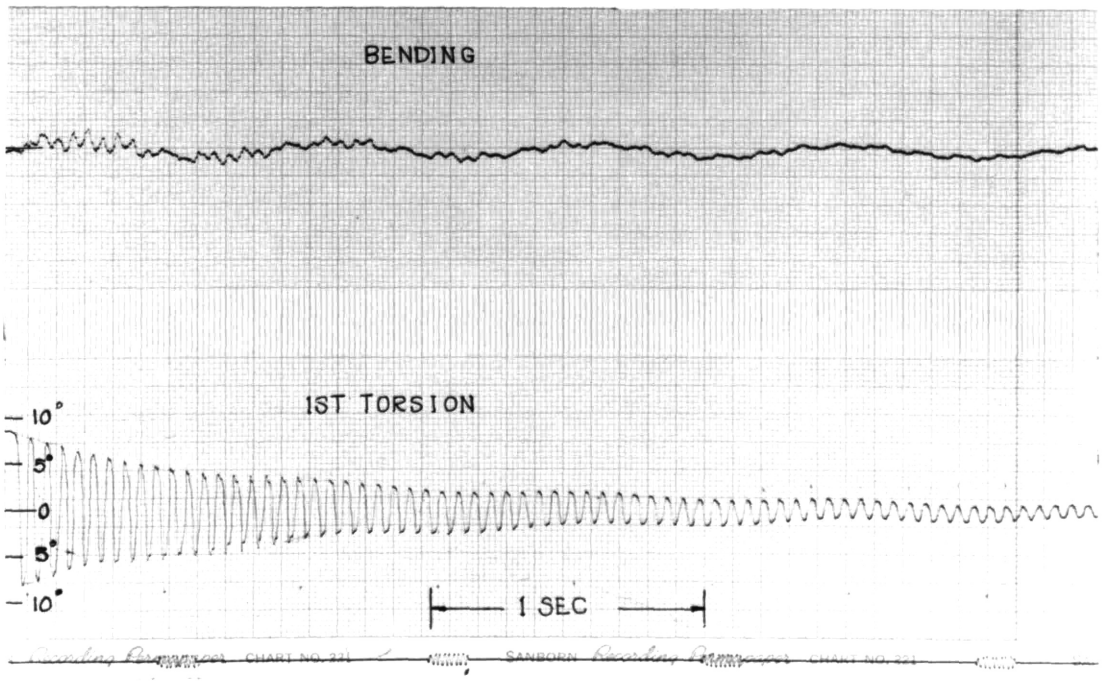

FIG. 13 SAMPLE FIRST TORSION DECAY RECORD

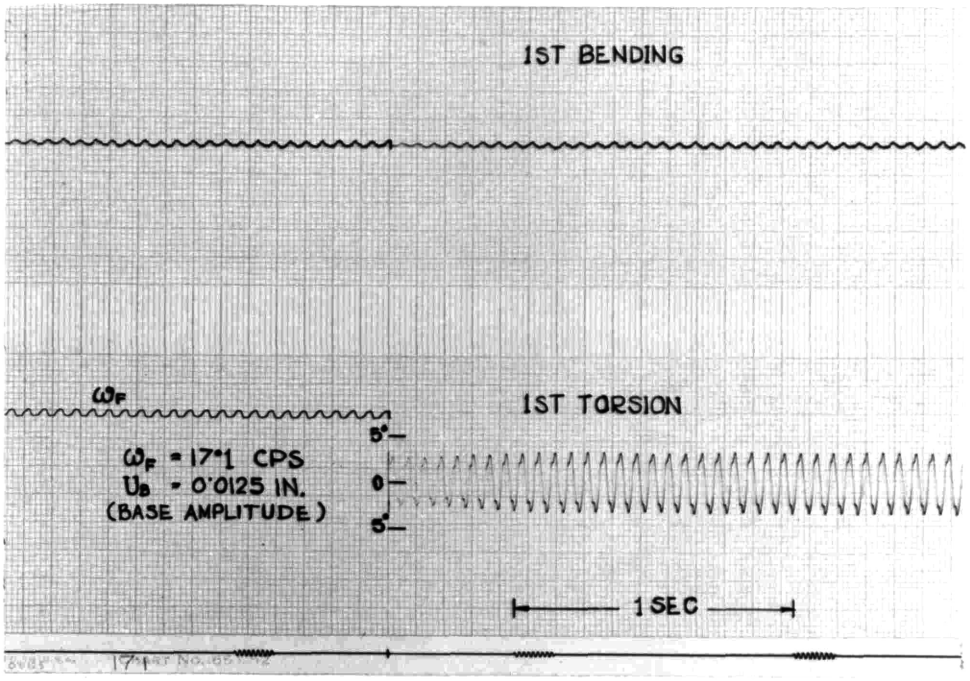

FIG. 14 STEADY STATE RESPONSE AT ω_F = 17.1 CPS

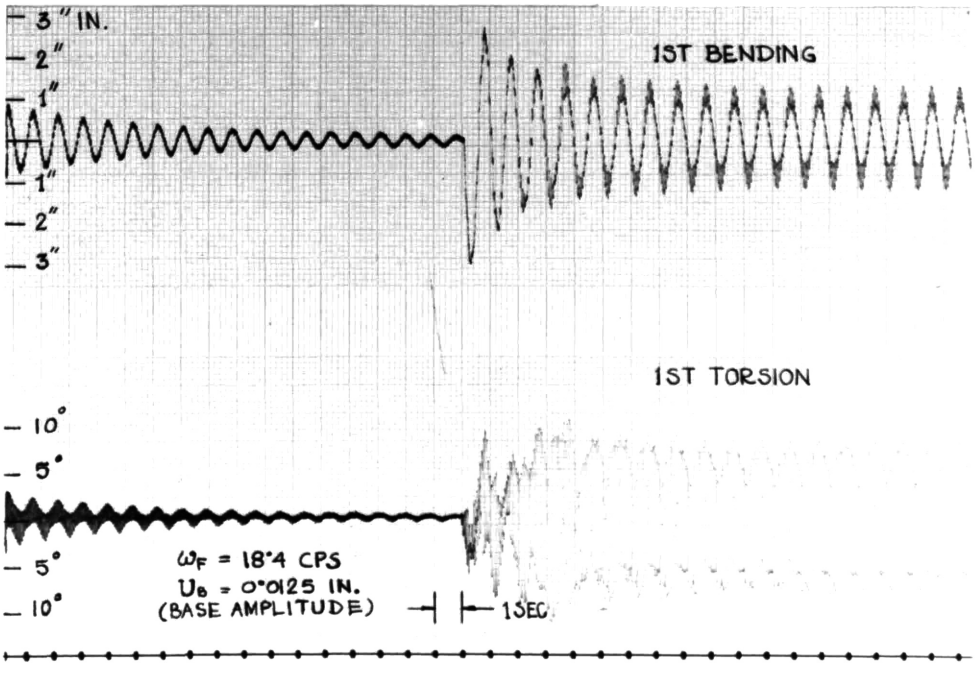

FIG. 15a RESPONSE WITH SMALL AND LARGE KICK AT ω_F = 18.4 CPS

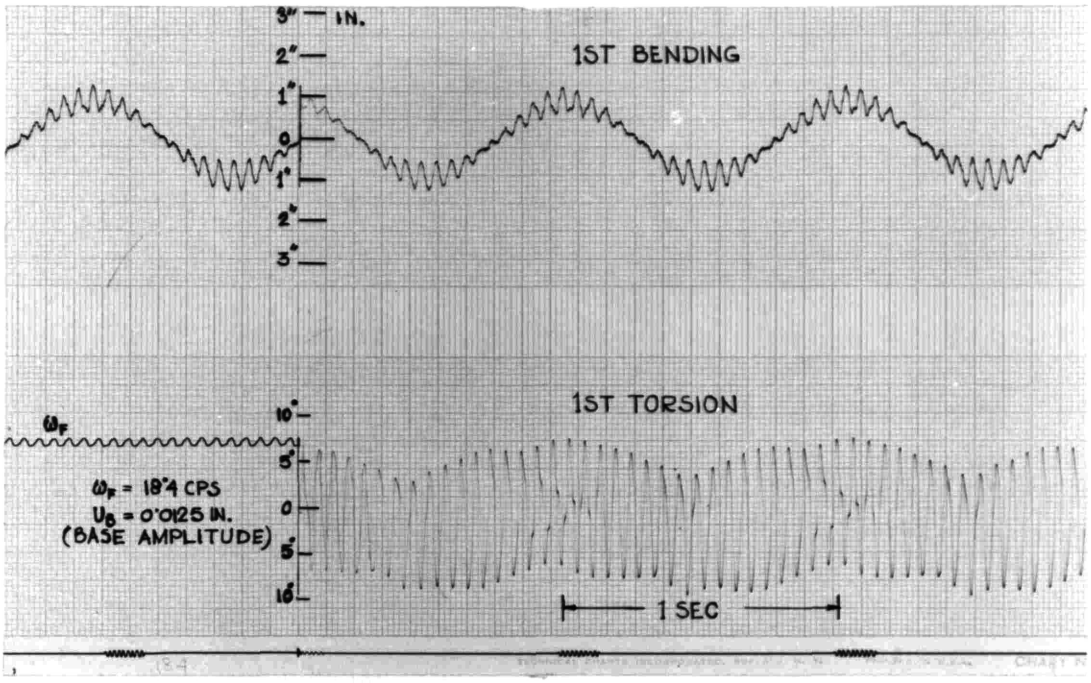

FIG. 15b LIMIT CYCLE RESPONSE AT $\omega_F = 18.4$ CPS

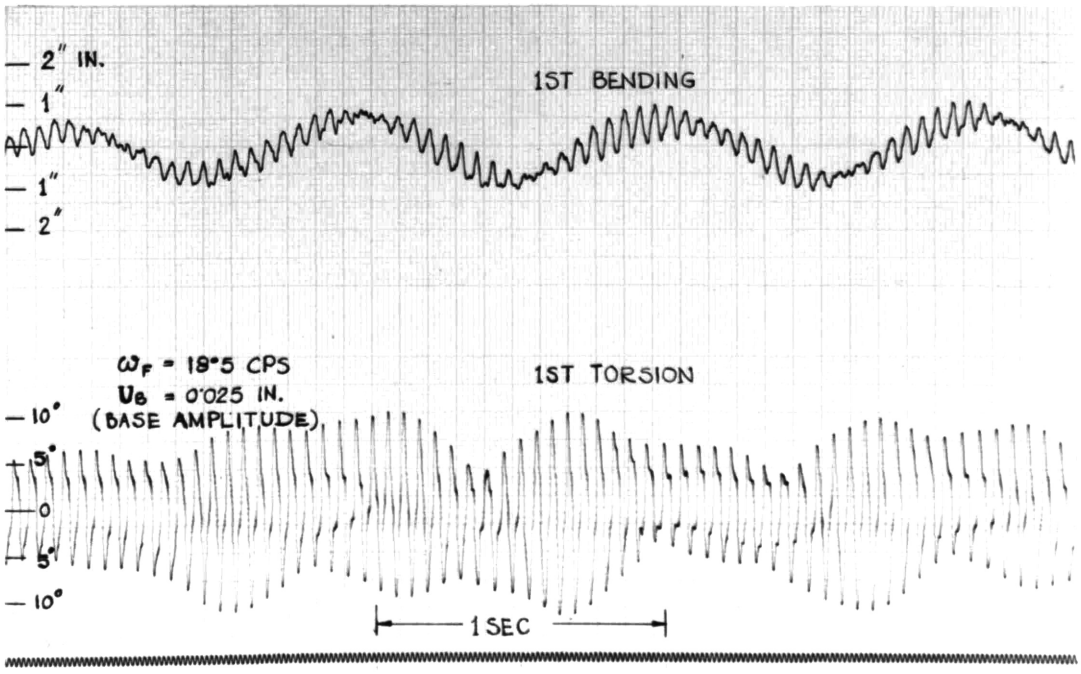

FIG. 15c LIMIT CYCLE RESPONSE AT $\omega_F = 18.5$ CPS

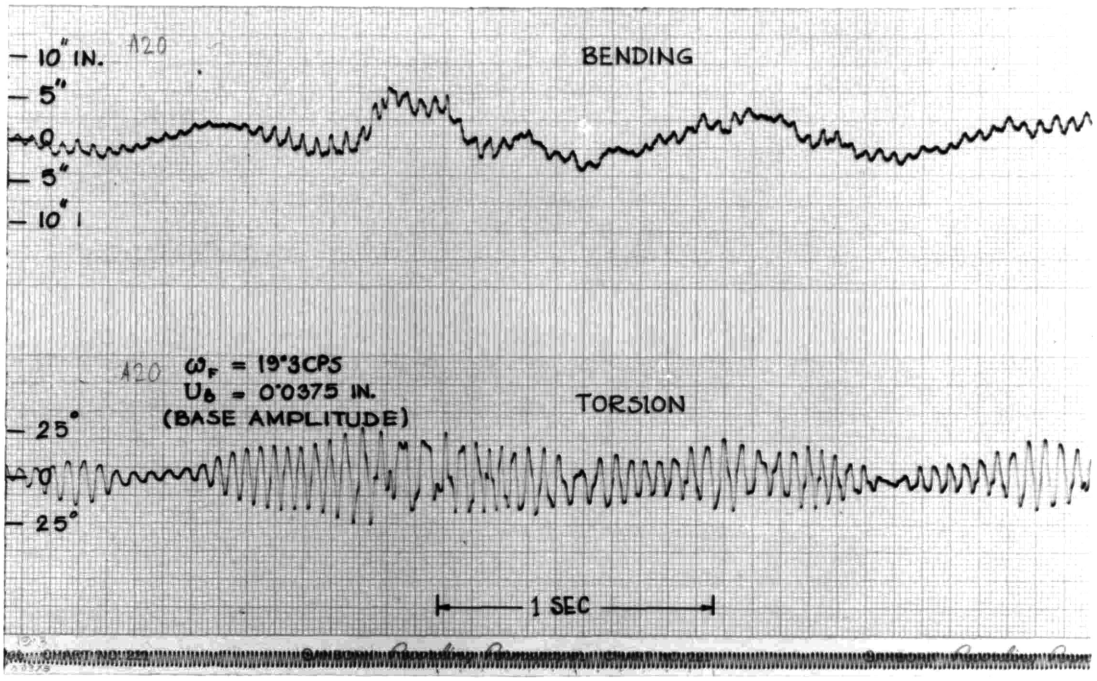

FIG. 15d RESPONSE WITH LIGHT KICK AT ω_F = 19.3 CPS

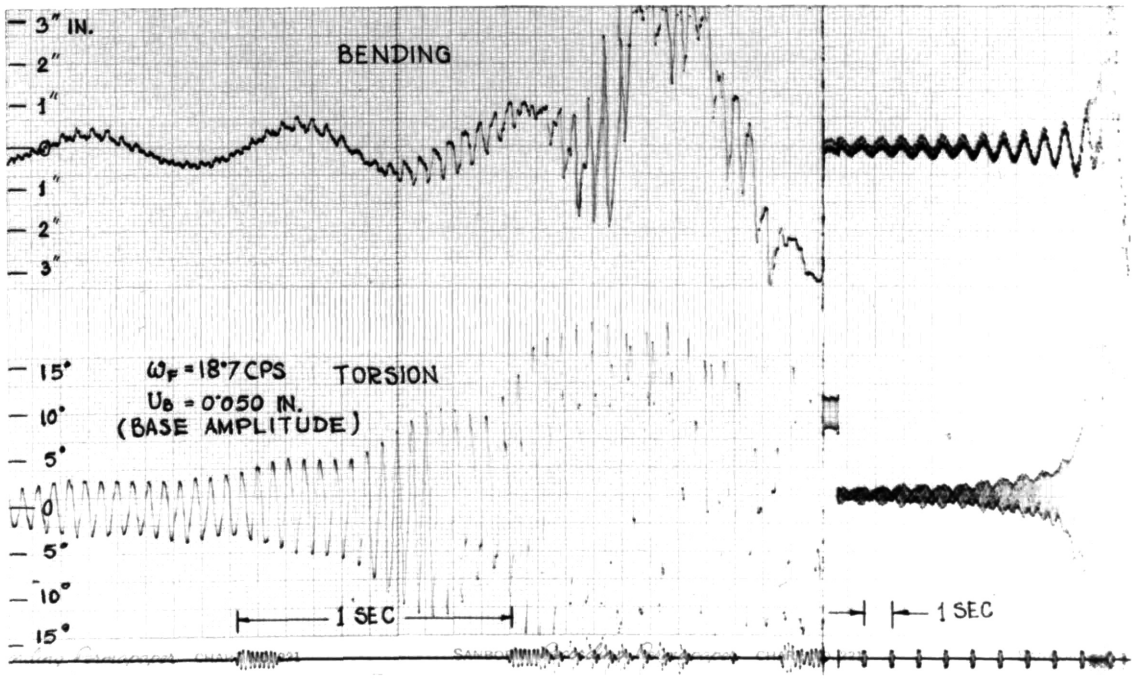

FIG. 15e SNAPPING WHEN RELEASED FROM REST AT ω_F = 18.7 CPS

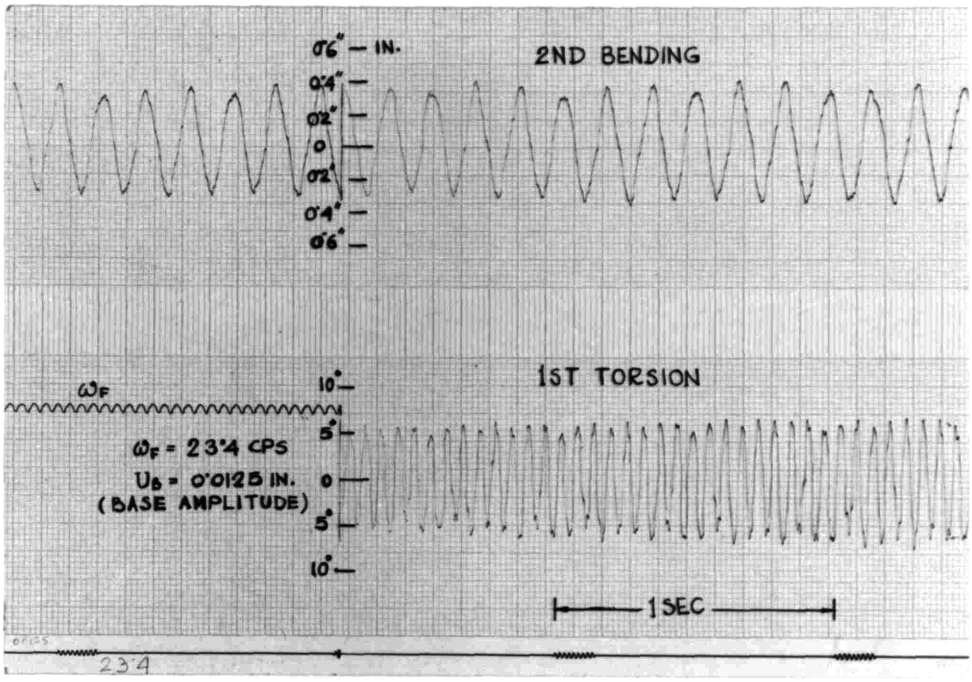

FIG. 16a STEADY STATE RESPONSE AT $\omega_F = 23.4$ CPS

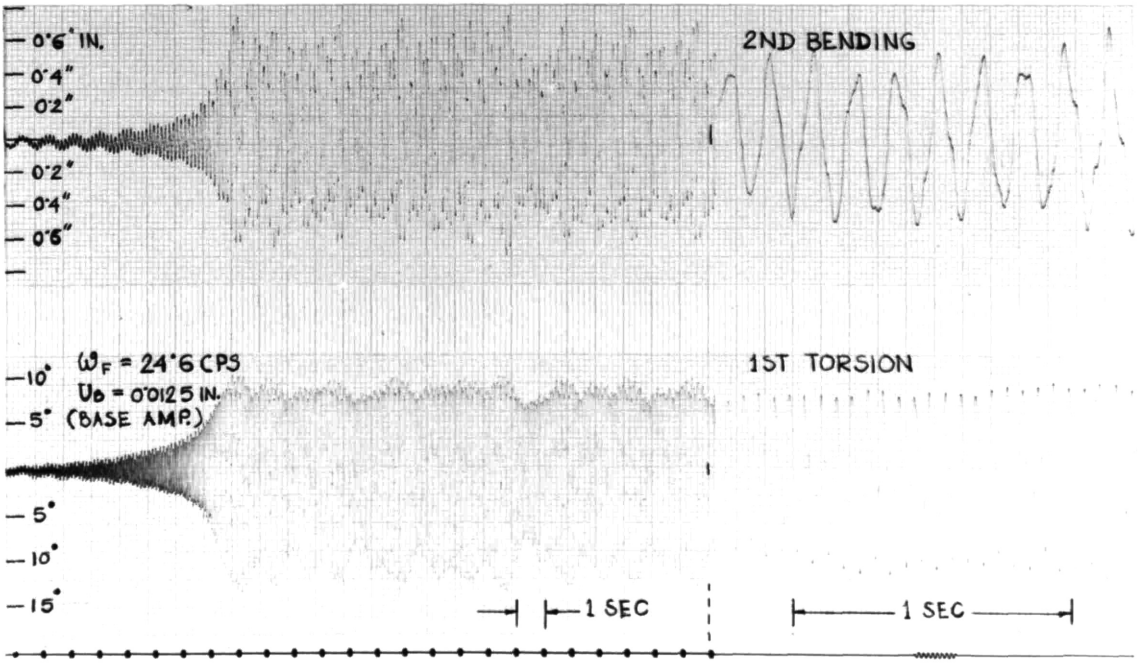

FIG. 16b LIMIT CYCLE RESPONSE AT $\omega_F = 24.6$ CPS

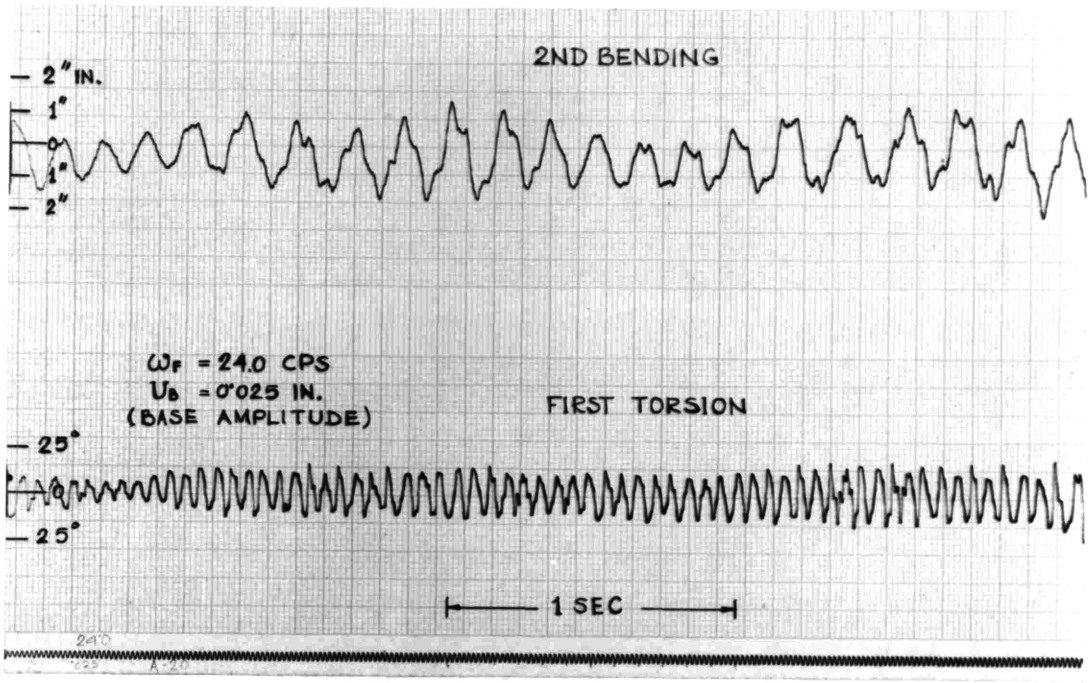

FIG. 16c RESPONSE AT ω_F = 24.0 CPS

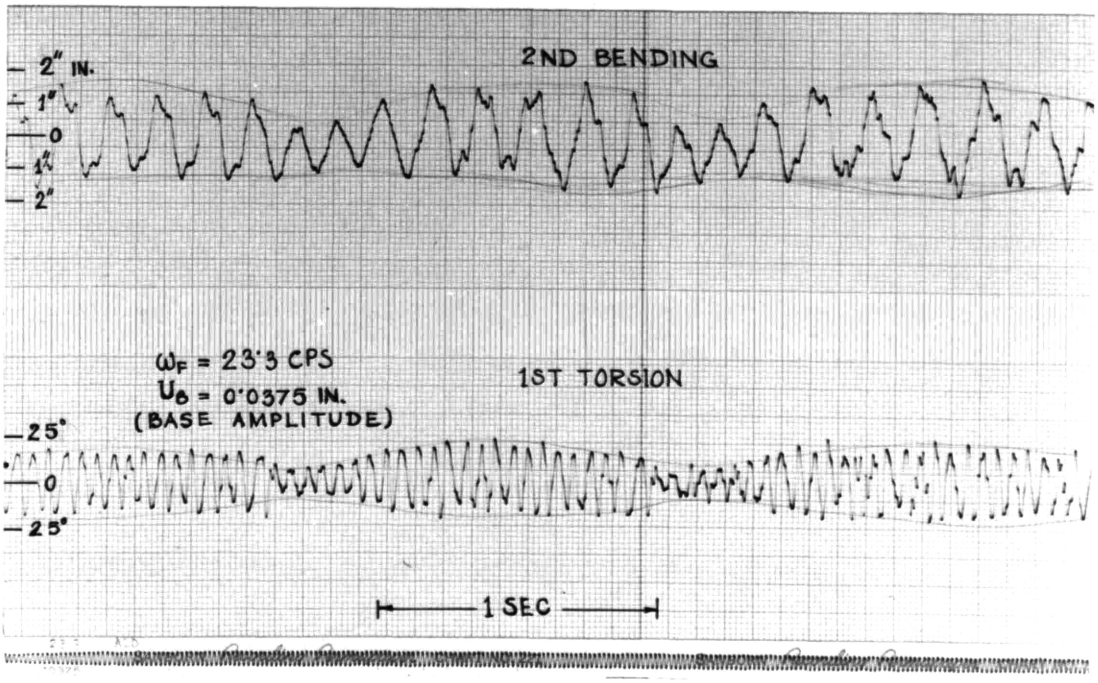

FIG. 16d BEATING RESPONSE AT ω_F = 23.3 CPS

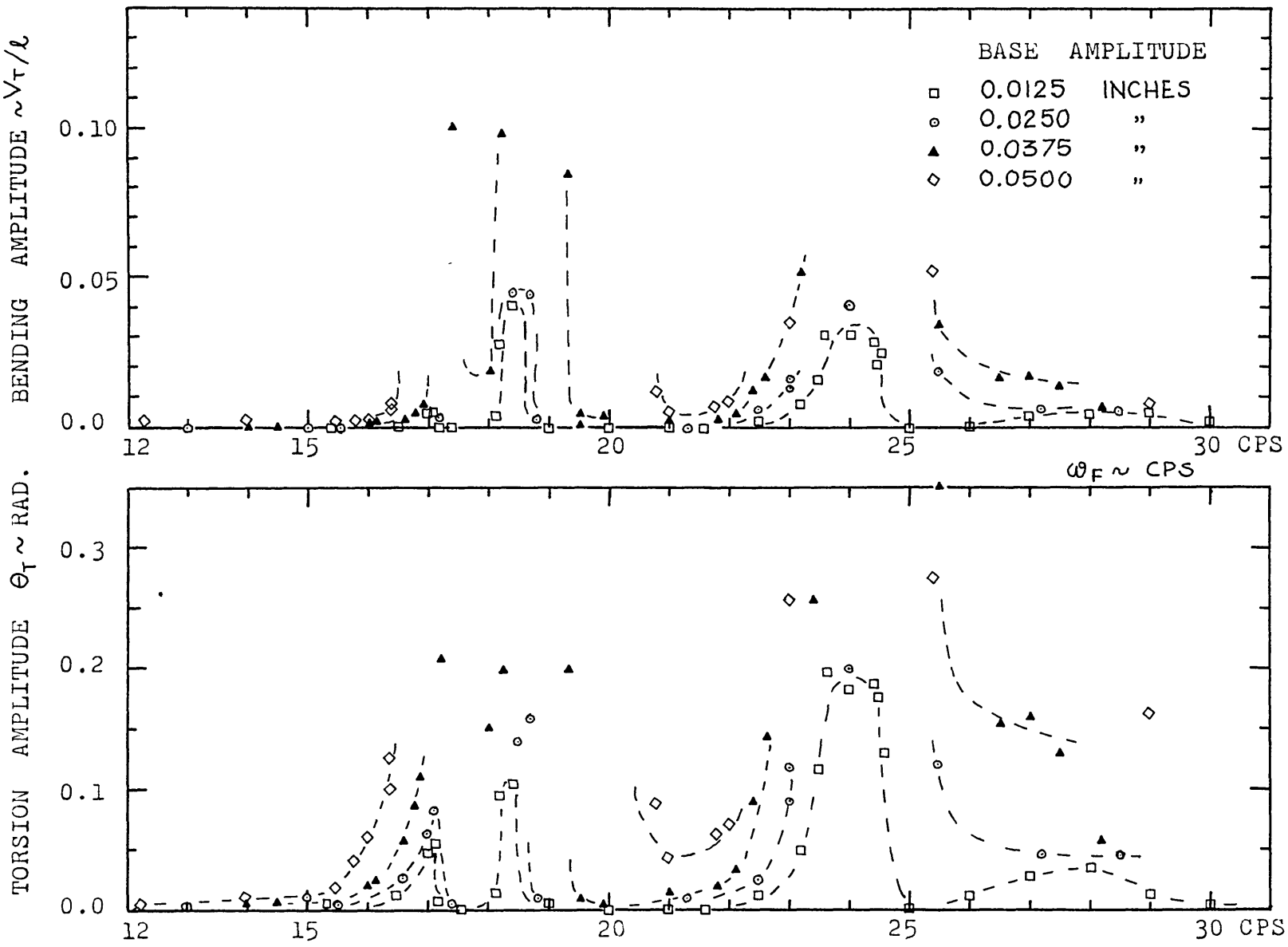

FIG. 17 AMPLITUDE RESPONSE VS. FORCING FREQUENCY W_F

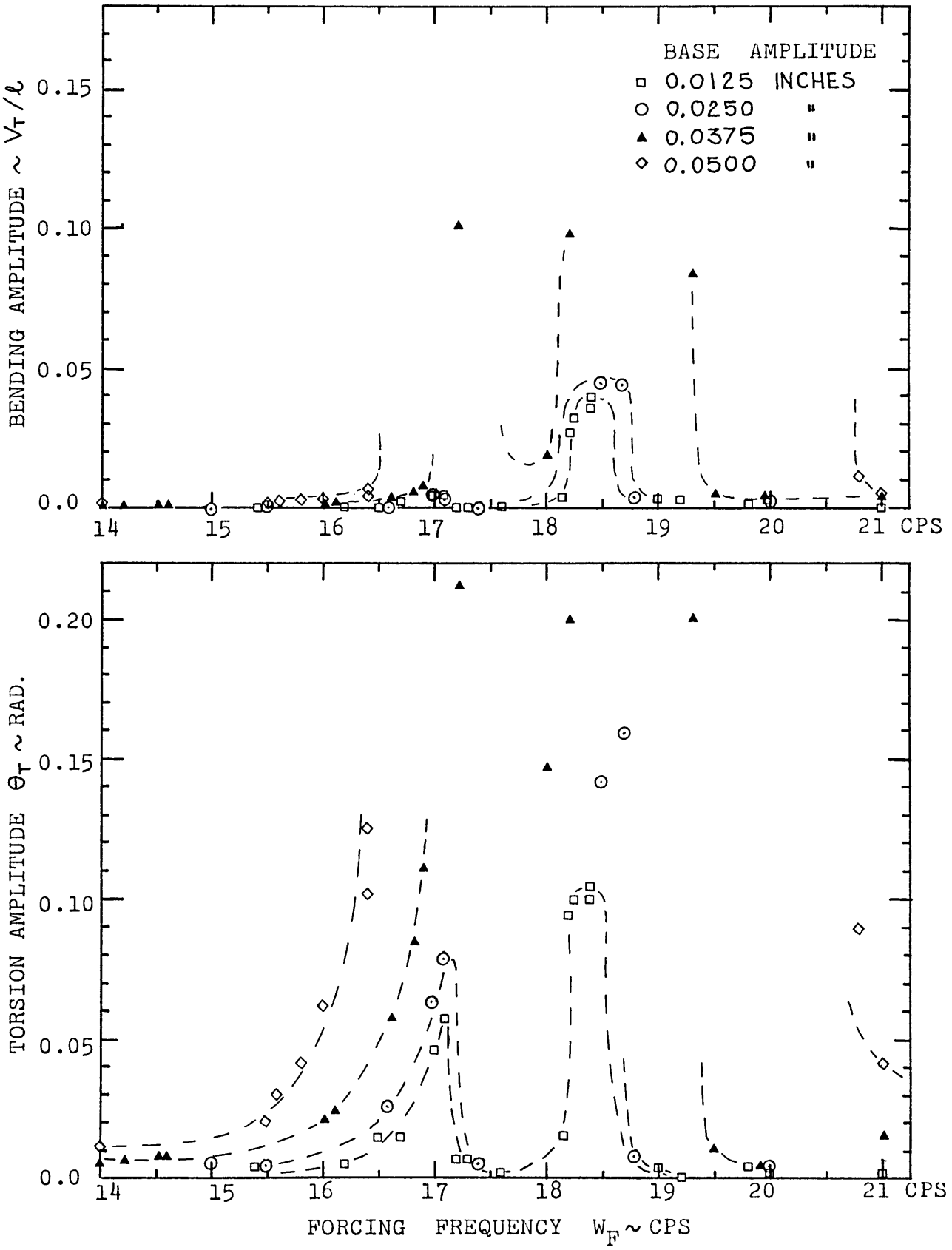

FIG. 18 AMPLITUDE RESPONSE (1ST BENDING AND 1ST TORSION)

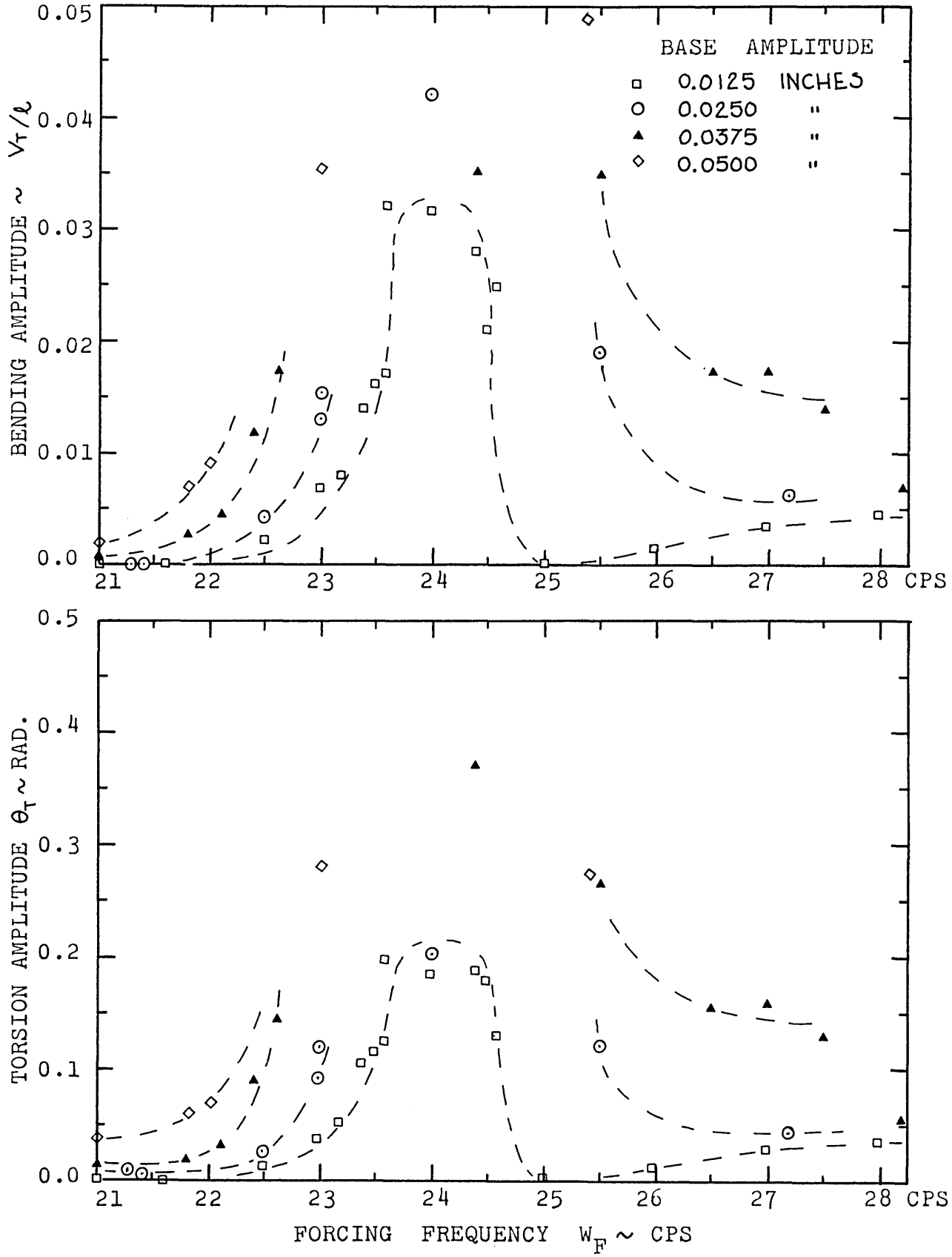

FIG. 19 AMPLITUDE RESPONSE (2ND BENDING AND 1ST TORSION)

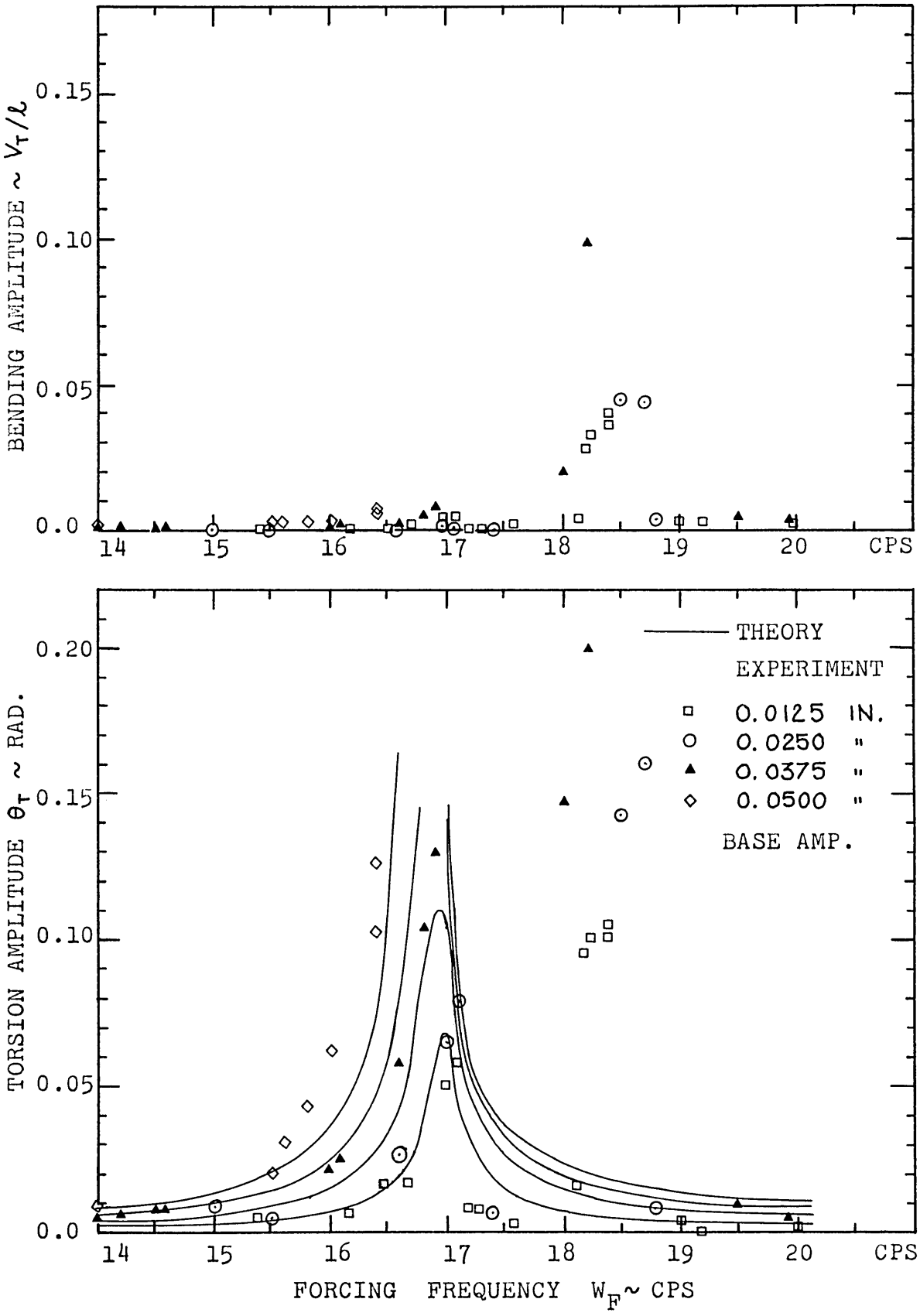

FIG. 20 THEORY AND EXPERIMENT COMPARISON